Atmos. Chem. Phys. Discuss.,
doi:10.5194/acp-2016-520-RC1, 2016

Interactive comment on "Lidar detection of high concentrations of ozone and aerosol transported from Northeast Asia over Saga, Japan" by Osamu Uchino et al.

The authors wish to thank two referees for helpful and thoughtful comments. Each comment is addressed individually below. The reference comments are written in black, and our responses are described in red.

The main changes of the paper since the original APCD versions are as follows:

- Figures were changed as follows: 1) Figs 3c, 4, and 7-11 were added, 2) Figs. 4 and 5 were replaced with Figs. 5 and 6, and 3) Fig. 6 was removed. In addition to these changes, the scale of Fig 3b was changed because total depolarization ratio was calculated only from the signal of the low sensitive P channel of which error was small.
- Fifteen references were added.
- Section 5 (Discussion and concluding remarks) was divided into two sections:
  5 Discussion: origin and transport pathways of ozone and aerosol plumes
  6 Concluding remarks

In the revised paper, the sentences moved from the original paper are written in blue. The original sentences in yellow highlighter with strikethrough were deleted in the revised paper. The original sentences with strikethrough were also deleted. The sentences added in the revised paper were written in red.

Anonymous Referee #1

Received and published: 26 July 2016

The paper by Uchino et al. presents lidar measurements of high ozone and aerosol concentrations over southern Japan and a comparison with models. Measurements and the model outputs are interesting and a complete analysis of these datasets is worth scientific publication. However, the current analysis of these datasets does not seem to fully exploit the information they provide and many statements are not clearly justified (even though the observational and modelling datasets to do it are potentially available already). I recommend the following major revisions:

1) Evidence on the origins (location and type of source) and transport pathways (particularly in the vertical) of the ozone and aerosol plumes are not clearly provided. Chemistry-transport model outputs are not exploited for this, as currently, simulations are only used for comparison with lidars. I recommend fully developing this aspect, with analysis of the model outputs at the scale of East Asia and in the vertical. This is very important to provide information on the horizontal and vertical pathways of the pollutant plumes and their origin (e.g. type of aerosols).

We provided information on the horizontal and vertical pathways of the pollutant plumes and their origin including the type of aerosols in the discussion in lines 345-356 and 352-365, and revised the abstract in lines 24-33as follows:

Lines 347-356:

Figure 7 shows the time-altitude cross sections of total aerosol extinction coefficients at 550 nm, and the ratios of dust extinction coefficients to total aerosol extinction coefficients simulated by MASINGAR-mk2 with potential temperatures over Saga for 20–31 March 2015. For the event on 22 March, the model predicted the dust particles (60–100%) in the altitude range 1–3 km, and sulfate (40–60%) and dust (30–40%) particles below 1 km. The number of the parenthesis represents the ratio of each component's extinction coefficient to the total extinction coefficient. The dust particles descended to the surface in the afternoon (Fig.7b). For the event on 30 March, MASINGAR mk-2 predicted the dust particles (50–100%) for 1–6 km, and sulfate (50–80%) and dust (0–20%) particles below 1 km in the morning. Mie lidar data support the model prediction because D_p is high (17 ± 6%) for 1–3 km and low (10 ± 3%) below 1 km. For both events, small amounts of organic carbon, black carbon and sea salt particles were predicted.

Lines 360-373:

An~~Twenty seven~~ air parcel~~s~~ was ~~were~~ initially left at altitudes of ~~600–1000~~ 1.500 m (Fig. 8a) and 500 m (Fig.9a) over the lidar site at Saga. The trajectories were calculated for three days from 21~~00~~:00 UTC ~~(09:00 JST)~~ on 21~~2~~ (06:00 JST on 22) March 2015. Figures 8b and 9b show the time-altitude cross sections of dust and sulfate extinction coefficients simulated by MASINGAR mk-2 along the trajectory paths of Figs. 8a and 9a respectively. Based on the results of the backward trajectories and the model simulations, the dust and sulfate particles ~~high ozone and aerosol concentrations~~ on 22 ~~and 31~~ March could have been transported within about two days from the Gobi Desert and the North China Plain (NCP), respectively~~the Northeast Asia~~. The highest concentrations of SO_2 and NO_2 in the world were observed in NCP for 2013–2015 by the Ozone Monitoring Instrument (OMI) onboard NASA's Aura satellite, as shown in Fig.5 by Krotkov et al. (2016). These gases are important precursors of sulfate particles and ozone. Figure 10 represents the horizontal maps of ozone volume mixing ratios at 925 hPa (about 760 m altitude) simulated by MRI-CCM2 at 21:00 JST on 19, 20, 21 March and at 03:00 JST on 22 March 2015. These maps indicate that the high ozone could be transported from NCP to the Yellow Sea and then Saga within about two days.

Abstract, lines 24-33:

Backward trajectory analysis and the simulations by the Model of Aerosol Species IN the Global AtmospheRe (MASINGAR) mk-2 and the Meteorological Research Institute Chemistry-Climate Model, version 2 (MRI-CCM2) indicated that the mineral dust particles originated from the Gobi Desert and an air mass with high ozone and aerosol (mainly sulfate) concentrations ~~could have been transported~~

originated from the North China Plain~~Northeast Asia~~ could have been transported over the measurement site within about two days. ~~Based on the lidar data and the ground-based in-situ measurements at Saga, this air mass could have been transported to the surface by vertical mixing when the planetary boundary layer developed in the daytime~~. These~~is plume, which contained~~ high ozone and aerosol ~~pollutant~~ concentrations~~,~~ impacted surface air quality substantially in the afternoon on 22 March 2015.
In accordance with these modifications, we added four figures (Figs.7–11) using the model outputs of HYSPLIT, MASINGAR-mk2 and MRI-CCM2, and lidar data.

2) Analysis of lidar data: the vertical structure of ozone and aerosol layers are not completely analysed, as the heights of the atmospheric boundary layer (mixing and residual layers) are not depicted. As shown in numerous papers, the detection of these layers may be easily done with the aerosol lidar. Such analysis should be added in the paper and precisely explain in a chronological order the mechanisms involved (i.e.vertical mixing, arrival of pollutants, etc).
We estimated the tops of the atmospheric boundary layers from the range-corrected backscatter signal at 1064 nm (Fig.11), and explained the arrival of pollutants (dust, sulfate and ozone) and their vertical mixing to the surface when the mixed layer developed in the afternoon in lines 383-400:

To investigate the vertical transport processes of the aerosol and ozone in the lower troposphere over the measurement site, we show in Figure 11 the time variations of the top altitudes of the atmospheric boundary layers from 11:10 JST on 20 March to 14:33 JST on 31 March 2015 which were estimated from the 1064 nm range-corrected backscatter signals with a range resolution of 15 m using the wavelet covariance transform method (Baars et al., 2008; Izumi et al., 2016), and those obtained from the radiosonde data at Fukuoka and the JMA Meso-scale Analysis (MA) data over Saga using the parcel method (Holzworth, 1964). When the mixed layers developed in the afternoon, the tops of the mixed layers (1.5–2 km) estimated by Mie lidar were almost consistent with those by MA. However, Mie lidar had a tendency to detect the residual layers in the night and morning time, e.g., 21–22 March although the radiosonde data at 9:00 JST on 22 March found the top of the mixed layer was 117 m (Stull, 1988), and it was difficult for Mie lidar to detect the mixed layer because the lowest altitude of the Mie lidar measurement was 225 m.

The dust particles originated from the Gobi Desert arrived at 1–3 km altitudes above the residual layer over the lidar site at 06:00 JST on 22 March. When the mixed layer developed to 1.5–2 km at 11:00–15:00 JST on 22, the dust particles were supposed to be mixed into the boundary layer and then reached the surface by the entrainment, as simulated in Fig.7b. This could result in the sharp increase in PM2.5 concentrations at the surface increased sharply after 11:00 JST, as shown in Fig.4. The similar phenomenon was observed over the northern Kyushu area during the dust event in late May–early June 2014 (Uno et al., 2016).

3) Technical characteristic of the datasets: in the presentation of the results, too much technical information of the datasets (instrument characteristics, model configuration, variables describing the

datasets, etc) is given. The geophysical interpretation of the measurements is relatively scarce. For sake of clearness for the readers, I recommend that most of technical remarks on the datasets are given a previous section dedicated to datasets characteristics and then only the geophysical interpretation is given when describing the figures.

We moved the remarks on the observation (formerly, physical) parameters obtained by Mie lidar and the vertical and time resolutions of Mie lidar and ozone DIAL data to Section 2.

4) The extinction-to-backscatter ratio : the climatological values that are used are expected to be suited to a particular type of aerosol (it changes a lot depending on the origin and size). What kind of aerosol is it for 50 sr at 532 nm? Measurements suggest the presence of large non-spherical particles (likely desert dust). How is this taken into account? I recommend using different extinction-to-backscatter ratios for each kind of particles (dust, sulphate, etc).

We corrected as follows:

Lnes 97-99:

We assumed the lidar ratio *LR* (extinction-to-backscatter ratio) for aerosols to be 50 sr at 532 nm and 45 sr at 1064 nm based on the lidar ratios for Asian dust and pollution aerosols summarized by Sakai et al. (2003), Anderson et al. (2003) and Cattrall et al. (2005).

Their summaries are as follows:

Sakai et al.(2003): Asian dust 47±18 sr,

Cattrall et al.(2005): Dust (spheroids) 42±4 sr, SE AsiaPollution 58±10 sr,

Anderson et al.(2003): ACE-Asia Pollution

(Fine-dominated, submicron portion) 50±5 sr, Dust (Coarse-dominated, Dust-like chemistry, Supermicron portion) 46±8 sr.

I recommend the following minor revisions:

1) English language should be revised in the whole the paper.

Before we submitted our manuscript to ACP, the manuscript had been edited carefully by two native-English-speaking professional editors from ELSS, Inc. (elss@elss.co.jp, http://www.elss.co.jp). In the revised paper, we made our efforts for the readers to understand it more clearly.

2) Colour scales in figure 2 should be changed in order to highlight changes from background.

We highlighted the high ozone event on 22 March 2015 in red color.

3) Line 93: what is the meaning of "The errors were equated to 100% times the lidar signal-to-noise ratios". Please clarify.

We changed the sentence as follows:

Line 151-152:

The errors were computed from the lidar signal-to-noise ratios by use of Poisson statistics.

4) Lines 106-108 : The justification of the following statement is not clear : "These observational results show the descent of regions of high ozone concentrations and suggest that air with high ozone concentrations was transported to the surface by vertical mixing when the planetary boundary layer developed during the daytime". What is the height of the boundary layer? This height should be clearly shown in the figures. When was it mixed? Which elements suggest a "descent" or downward mixing of the high ozone plume? This should be thoroughly explained and justify. The model may be used to describe this mixing mechanism. When it is mentioned “daytime” vertical mixing, it is in which day? In which location vertical occurs? The current explanation is very scarce and unclear. This should be thoroughly explained and justify.

We deleted the sentence of "These observational results show the descent of regions of high ozone concentrations and suggest that air with high ozone concentrations was transported to the surface by vertical mixing when the planetary boundary layer developed during the daytime" in Section 3. Instead, we discussed on this matter in Section 5 using Figs. 11.

Lines 383-400:

To investigate the vertical transport processes of the aerosol and ozone in the lower troposphere over the measurement site, we show in Figure 11 the time variations of the top altitudes of the atmospheric boundary layers from 11:10 JST on 20 March to 14:33 JST on 31 March 2015 which were estimated from the 1064 nm range-corrected backscatter signals with a range resolution of 15 m using the wavelet covariance transform method (Baars et al., 2008; Izumi et al., 2016), and those obtained from the radiosonde data at Fukuoka and the JMA Meso-scale Analysis (MA) data over Saga using the parcel method (Holzworth, 1964). When the mixed layers developed in the afternoon, the tops of the mixed layers (1.5–2 km) estimated by Mie lidar were almost consistent with those by MA. However, Mie lidar had a tendency to detect the residual layers in the night and morning time, e.g., 21–22 March although the radiosonde data at 9:00 JST on 22 March found the top of the mixed layer was 117 m (Stull, 1988), and it was difficult for Mie lidar to detect the mixed layer because the lowest altitude of the Mie lidar measurement was 225 m.

The dust particles originated from the Gobi Desert arrived at 1–3 km altitudes above the residual layer over the lidar site at 06:00 JST on 22 March. When the mixed layer developed to 1.5–2 km at 11:00–15:00 JST on 22, the dust particles were supposed to be mixed into the boundary layer and then reached the surface by the entrainment, as simulated in Fig.7b. This could result in the sharp increase in PM2.5 concentrations at the surface increased sharply after 11:00 JST, as shown in Fig.4. The similar phenomenon was observed over the northern Kyushu area during the dust event in late May–early June 2014 (Uno et al., 2016).

5) Line 120: The sentence "The most reasonable results were obtained when the following changes were made (Fig. 2b)" does not seem to match the Figure as it does not explain the changes in the model, but it

presents the final results.

We changed the sentence in lines 181-183:

However, the MRI-CCM2 predicted the high ozone concentrations of 50–60 ppbv and could not reproduce those ~~the high ozone concentrations~~ of 90–110 ppbv observed below an altitude of 1.5 km during 03:00–20:00 JST on 22 March 2015.

6) Line 130: there is also a difference in the time of the arrival of the plume. Please, report.

We added the following sentence to lines 194-195:

And the MRI-CCM2 predicted the high ozone concentration a half day earlier than the DIAL observation.

7) The term "bad weather" is not objective. I suggest to use "rainy" conditions or similar.

We used “rainy and cloudy conditions”.

8) The wavelength exponent, Alp : the name to this variable does not seem very conventional. For optical depth, the term "Angström exponent" is usually used in literature. The name Â´n wavelength exponent Â˙z does not seem very explicit. Why the symbol is "Alp" ? Is this term often used by the scientific community?

As suggested by the referee, the term " Ångström exponent" is usually used for optical depth in literature. Therefore we use “The backscatter-related Ångström exponent *Alp*” for backscattering coefficient (line 115-116).

9) Line 167 : The term "always existed" is not clear. Does it mean that it is observed in the timeseries shown in Figure 3 ? Please, clarify.

We added “for 20–31 March 2015” (lines 251-252).

10) What is the effect of aerosols in the ozone DIAL measurements ? What are the possible biases that they might induce ? Please provide an estimation of this bias for the cases of very high aerosol concentrations shown in Fig 3 on 22 March 2015.

We added the following sentences in lines 196-204:

The maximum bias (systematic error) of ozone DIAL data caused by aerosols was estimated to be 20% (15 ppbv) at 0.57 km, and the mean bias and the standard deviation were 7% ± 5% in the altitude range 0.57–2.0 km at 11:00 JST. These biases were estimated from *Alp* observed at the same time by Mie lidar and assuming *LR* =50 sr in the wavelength range 276–299 nm, based on the equations of (6) and (7) in Uchino and Tabata (1991). These biases were not large since the 276/287 nm and 287/299 nm wavelength pairs were suitable for measurements of ozone in the boundary layer and the free troposphere respectively (Nakazato et al., 2007). As mentioned earlier, the ozone DIAL data with the statistical error smaller than 10% was used in this study. Therefore the uncertainty of the ozone DIAL data was estimated to be smaller than 22% and the mean value of the uncertainty was 12%.

11) Line 170 : What is the scientific evidence that suggest that small particles in the event of 22 March 2015 are "sulphate" particles ? This should be clearly justified.

Because we did not make the in-situ measurement of aerosol component, we deleted the word “sulfate” from the text (line 257). However, the model predicted that the particles were mostly sulfate.

12) Lines 174-181: Surface measurement of PM2.5 should be presented in the figure. A literal description seems insufficient. Please, add the time series of theses measurements.

We added “Fig.4” to show hourly data of surface PM2.5 and Ox at Takagimachi, Saga for 20-31 March 2015.

13) Section 4.1: the model should be use to identify the type and origin of the aerosols.

We used the model to identify the type and origin of the aerosols. The results were presented in Figs. 7, 8 and 9 and the explanation was provided lines 347-367:

Figure 7 shows the time-altitude cross sections of total aerosol extinction coefficients at 550 nm, and the ratios of dust extinction coefficients to total aerosol extinction coefficients simulated by MASINGAR-mk2 with potential temperatures over Saga for 20–31 March 2015. For the event on 22 March, the model predicted the dust particles (60–100%) in the altitude range 1–3 km, and sulfate (40–60%) and dust (30–40%) particles below 1 km. The number of the parenthesis represents the ratio of each component’s extinction coefficient to the total extinction coefficient. The dust particles descended to the surface in the afternoon (Fig.7b). For the event on 30 March, MASINGAR mk-2 predicted the dust particles (50–100%) for 1–6 km, and sulfate (50–80%) and dust (0–20%) particles below 1 km in the morning. Mie lidar data support the model prediction because D_p is high (17 ± 6%) for 1–3 km and low (10 ± 3%) below 1 km. For both events, small amounts of organic carbon, black carbon and sea salt particles were predicted.

To identify the origin of the ~~ozone and~~ aerosols and related transport processes, three-dimensional backward trajectories of air parcels were calculated with the NOAA Hybrid Single Particle Lagrangian Integrated Trajectory (HYSPRIT) model (Draxler and Hess, 1998; Stein et al., 2015)~~., as shown in Fig. 6.~~ An~~Twenty seven~~ air parcel~~s~~ was ~~were~~ initially left at altitudes of ~~600–1000~~ 1500 m (Fig. 8a) and 500 m (Fig.9a) over the lidar site at Saga. The trajectories were calculated for three days from 21~~00~~:00 UTC ~~(09:00 JST)~~ on 21~~2~~ (06:00 JST on 22) March 2015. Figures 8b and 9b show the time-altitude cross sections of dust and sulfate extinction coefficients simulated by MASINGAR mk-2 along the trajectory paths of Figs. 8a and 9a respectively. Based on the results of the backward trajectories and the model simulations, the dust and sulfate particles ~~high ozone and aerosol concentrations~~ on 22 ~~and 31~~ March could have been transported within about two days from the Gobi Desert and the North China Plain (NCP), respectively, to the measurement site ~~the Northeast Asia~~.

14) Line 208: the term "AODs were almost the same" is only approximate. Objective

terms should be used. Mean bias and RMS differences should also be given.

We added the following sentence in lines 307-309:

The mean bias and the standard deviation of AOD between Mie lidar and sky radiometer was 0.029 ± 0.051, and that between MASINGAR mk-2 and sky radiometer was –0.07 ± 0.24 for 20–31 March, except for 12:00–14:00 on 22 March.

15) Trajectory analysis: Timing in the comparisons does not seem to be precise enough. The ozone and aerosol plume arriving to Saga lasts for a few hours only. This cannot be justified with high ozone and aerosol concentration during a large period of time (e.g. March 2015). These airmasses arriving to Saga on 22 March were likely located near the Beijing area on which date precisely? On that date, where ozone and aerosol concentrations high?

We added the following sentence in lines 374-375:

Because it was difficult to obtain observational data of surface ozone and sulfate particles in NCP including Beijing on 19-20 March, we refer to the following papers related to those data.

16) Lines 237-238: The justification of this statement "Based on these lidar data and the in-situ measurement data at Takagimachi in Saga city, an air mass with high ozone and aerosol concentrations could have been transported from the free troposphere" is not clear to me. The high concentrations are observed in the lidar time series below 1.5 km. There is not indication that transport of pollutants only occurs in the free troposphere, given that the top of the boundary layer is usually near 1.5 km. What evidence is given that transport does not occur in the boundary layer or both in the free troposphere and the boundary layer? What is the height of the mixing boundary layer (during, the day, the night, in the region). The altitude of the back-trajectories should also be given.

We estimated the tops of the atmospheric boundary layers from the range-corrected backscatter signal at 1064 nm (Fig.11), and explained the arrival of pollutants (dust, sulfate and ozone) and their vertical mixing to the surface when the mixed layer developed in the afternoon in lines 383-404 (The texts were given in the response to the referee's comment 4).

Atmos. Chem. Phys. Discuss.,
doi:10.5194/acp-2016-520-RC2, 2016

Interactive comment on "Lidar detection of high concentrations of ozone and aerosol transported from Northeast Asia over Saga, Japan" by Osamu Uchino et al.

Anonymous Referee #2

Received and published: 5 August 2016

Review of ACPD manuscript

The manuscript submitted to ACPD presents continuous lidar measurements of ozone and aerosol extinction at 532 and 1064 nm during 11 days over Southern Japan. The data are compared with two

Japanese global models: MRI-CCM2 for ozone and MASINGAR-mk2 for aerosol. The analysis of this long lidar data set is worth publication. However the goals of the paper are not well established and as already noticed by reviewer 1 the interpretation does not provide enough details to be very useful. There are already many publications reporting high ozone episodes measured with lidar techniques and a new paper on this topic has to go beyond existing literature. I see two ways: either to make a complete use of the long record and the vertical information available in the lidar data (e.g. comparing the 21-23 March with the 30-31 March ozone episode) or a true validation exercise of the models. In the present version neither option is really developed. As suggested by reviewer 1, a focus on the vertical transport during the high ozone episode using planetary boundary layer (PBL) development from the Mie lidar and temporal evolution of the modelled plumes may be a good option. Comparison of the March 21-23 with the March 30-31 ozone episode could be also interesting because the aerosol properties look different and the AOD on March 30 is less than the very large AOD seen on March 22. If the model assessment is the preferred option, then proper metrics used in papers discussing model accuracy have to be applied (e.g. see AEROCOM web site). Statistical parameters to quantify the quality of the simulation (mean bias, RMSE, normalized mean bias, etc...) and a discussion of all the possible model error sources must be provided. Therefore I propose a major update of the paper in either direction to avoid having just another report of a high ozone episode seen by a lidar.

The authors wish to thank the referee for helpful and thoughtful comments. In accordance with the referee's comment, we present the comparison of the March 22 with the March 30 episode because the aerosol properties look different and the AOD on March 30 is less than the very large AOD seen on March 22. To describe this, we added the following sentences in lines 347-356:

Figure 7 shows the time-altitude cross sections of total aerosol extinction coefficients at 550 nm, and the ratios of dust extinction coefficients to total aerosol extinction coefficients simulated by MASINGAR-mk2 with potential temperatures over Saga for 20–31 March 2015. For the event on 22 March, the model predicted the dust particles (60–100%) in the altitude range 1–3 km, and sulfate (40–60%) and dust (30–40%) particles below 1 km. The number of the parenthesis represents the ratio of each component's extinction coefficient to the total extinction coefficient. The dust particles descended to the surface in the afternoon (Fig.7b). For the event on 30 March, MASINGAR mk-2 predicted the dust particles (50–100%) for 1–6 km, and sulfate (50–80%) and dust (0–20%) particles below 1 km in the morning. Mie lidar data support the model prediction because D_p is high (17 ± 6%) for 1–3 km and low (10 ± 3%) below 1 km. For both events, small amounts of organic carbon, black carbon and sea salt particles were predicted.

Detailed comments

Introduction

A lot of details are given on GOSAT satellite validation which is not the scope of the paper. Line 60 Provide references about previous work dealing with high ozone episode measured by lidar: Kuang et al. Atmos. Env. 2011, Banta et al. JGR 1998, Eisele and Trickl Appl.Optics 2005, Ancellet et al. Atmos.Res.

2005, Kourtidis et al. JGR 2002, ... I believe none of these papers have published an 11-day continuous record so the advantage of your data set could be better presented in the introduction.

We added the following sentences in lines 69-72:

High ozone episodes in the lower troposphere have been observed by lidar (Banta et al., 1998; Koutidis et., 2002; Ancellet et al., 2005; Eisele and Trickl, 2005; Kuang et al., 2011). These observation records were limited to one week at most. We made an 11-day continuous record on 20–31 March 2015.

Section 2

Technical details about the lidar system are already given in Uchino 2012 and 2014 so it can be shortened, and alternatively provide the measurements characteristics (vertical and temporal resolution, range for the different wavelengths, specific aerosol corrections, lowest measurement range . . .). Are the ozone concentrations really given with 7.5 m and 1 min resolution ?

As suggested, we revised the texts in lines 135-139 as follows:

The 276/287 nm and 287/299 nm wavelength pairs were used for ozone DIAL measurements in the altitude ranges of 0.57–2.0 km and 2.0–6.0 km, respectively. The effective vertical resolutions were 270 m for 0.57–2.0 km and 540 m for 2.0–6.0 km, respectively (Uchino et al., 2014). The time resolution was set to 1 h to facilitate comparison with the MRI-CCM2. The aerosol correction was not made for the ozone retrieval.

Section 3

line 93 Be more precise about the criteria used to remove data affected by aerosols or clouds. Do you apply any aerosol corrections before this quality check ? If yes describe this correction. If not how large will be the bias in the ozone retrieval with a AOD larger than 1 at 532 nm as seen on March 22 ?

The criterion was added in lines 152-154:

Regions surrounded by a black rectangle are areas where the data were affected by aerosols and/or clouds with R larger than 2 at 299 nm, which were calculated assuming LR=50 sr without correcting attenuation by ozone absorption.

We did not apply any aerosol corrections, and so added the following sentence in lines 138-139:

The aerosol correction was not made for the ozone retrieval.

For the bias of ozone DIAL data, we added the following sentences in 196-204:

The maximum bias (systematic error) of ozone DIAL data caused by aerosols was estimated to be 20% (15 ppbv) at 0.57 km, and the mean bias and the standard deviation were 7% ± 5% in the altitude range 0.57–2.0 km at 11:00 JST. These biases were estimated from Alp observed at the same time by Mie lidar and assuming LR =50 sr in the wavelength range 276–299 nm, based on the equations of (6) and (7) in Uchino and Tabata (1991). These biases were not large since the 276/287 nm and 287/299 nm wavelength pairs were suitable for measurements of ozone in the boundary layer and the free troposphere respectively

(Nakazato et al., 2007). As mentioned earlier, the ozone DIAL data with the statistical error smaller than 10% was used in this study. Therefore the uncertainty of the ozone DIAL data was estimated to be smaller than 22% and the mean value of the uncertainty was 12%.

line 94 Define Ox. I understand why Ox is useful to discuss photochemistry in NO2 rich environment, but why not reporting surface ozone in Figure 2 ?
We mentioned as follows in lines 158-160:
Because the contribution of other components such as peroxyacetyle nitrate (PAN) to oxidant concentrations was extremely low, the oxidant volume mixing ratio was considered to be that of ozone.

line 103 The daily cycle which is clearly seen in surface Ox measurements is hardly visible in the lidar record even at the lower bound near 500 m. What is the reason for this ? Is the nocturnal PBL always lower than the lidar measurement range ?
We detected the low ozone concentrations in the nighttime on 10–11 January 2013, but the daily cycle of ozone was not detected at the lower bound near 600 m in this DIAL observation record. The daily cycle of ozone predicted by MRI-CCM2 was clear at least up to 250 m but not clear at 600 m. Therefore we are interested in the DIAL system which can measure ozone in the altitude range 100–500 m.

Line 106. This statement is not supported by any analysis. At least references must be given to support such a statement and all the observational evidence must be provided to validate this hypothesis.
In accordance with the reviewer's comment, the statement was deleted from Section 3. Instead we presented the related lidar observation results, the model output of MASINGAR-mk2, and the references in Discussion.

Line 126. What the uncertainty of the DIAL ozone data ? The discrepancy between the model O3 concentrations and the lidar data is very large (> 100%) which is generally well simulated by model (mean bias usually less than 50%). This should be discuss with more details to attribute the bias either to uncertainties in the data or to model error. Could you quantify the uncertainty related to the emission inventory ?
For the bias of ozone DIAL data, we added the following sentences in 196-204:
The maximum bias (systematic error) of ozone DIAL data caused by aerosols was estimated to be 20% (15 ppbv) at 0.57 km, and the mean bias and the standard deviation were 7% ± 5% in the altitude range 0.57–2.0 km at 11:00 JST. These biases were estimated from *Alp* observed at the same time by Mie lidar and assuming *LR* =50 sr in the wavelength range 276–299 nm, based on the equations of (6) and (7) in Uchino and Tabata (1991). These biases were not large since the 276/287 nm and 287/299 nm wavelength pairs were suitable for measurements of ozone in the boundary layer and the free troposphere respectively (Nakazato et al., 2007). As mentioned earlier, the ozone DIAL data with the statistical error smaller than 10% was used in this study. Therefore the uncertainty of the ozone DIAL data was estimated to be smaller

than 22% and the mean value of the uncertainty was 12%.

For the uncertainty of the inventory of sulfur dioxide (SO_2), we added the following sentences in lines 320-327:

Grainer et al.(2011) collected various emission inventories and compared them in global scales. They found that differences in Chinese sulfur dioxide (SO_2) emissions in 2000 reached 66% between the lowest and highest emissions and concluded that there was no consensus among the different inventories for the emissions of Chinese SO_2. This large variation among the inventories indicates that estimate of SO_2 emission in China has large error. In their comparison, the MACCity emission which was used in MASINGAR-mk2 simulation, showed the lower amount of Chinese SO_2 emission among the inventories. This fact might be responsible for the underestimation of pollution aerosol (sulfate) concentrations.

Section 4

line 139 What is the reference altitude where molecular scattering can be assumed ? On March 22 aerosol layers are seen up to 6 km and the Fernald inversion may be biased. This point must be addressed in the paper.

We added the following sentences in lines 311-315:

One possible reason for the large difference in AOD (~0.2) between Mie lidar and Sky radiometer data is that we set the reference altitudes 8.2 km and 2.8 km at 12:00 and 13:00 JST on 22 March, respectively, for the lidar because the backscattered signals were strongly attenuated by the dense aerosol layers below 2 km. This might cause the large differences of AODs between Mie lidar and sky radiometer data.

Line 140 Lidar ratio may change from 70 sr for pollution aerosol to 30 sr for dust or marine aerosol. What is the reason for choosing 50 sr ? Of course it is likely to increase again the model underestimate of the extinction on March 22 if you apply 70 sr. What are the lidar ratio values assumed in the model simulation ?

The lidar ratio *LR* is not used in the MASINGAR-mk2 because the extinction coefficient is calculated directly from the size distribution and the refractive index of each aerosol component.

Line 155 I assume the authors are using the 1064 backscatter ratio to calculate the wavelength exponent alp but the error is generally large for the inversion in the IR. What is the expected error on alp ? How does this exponent change for the different layers observed in the lidar record.

We added the following sentences in lines 260-264:

When there were no clouds above, *R* at 1064 nm was estimated assuming *Alp*=1.5 at the reference altitude where very small amount of aerosols was expected to be present, i.e., R=1.06 ± 0.06 (D=1.2 ± 0.51) at 532 nm, in the altitude range 3–6 km. If the value of *Alp* was changed from 1.0 to 2.0 at the reference altitude, the uncertainty in *Alp* was estimated to be ± 0.2. Alp was 0.3–2.0 in the 11-day Mie lidar record.

Line 169 and 171 Provide error bar on the depolarization ratio and wavelength exponent.

We added the error bar (one standard deviation) on the depolarization ratio and wavelength exponent in lines 252-265:

An event of high aerosol loading with large values of R (>8~~4–19~~) was observed below altitudes of 1.5 km for 03:00–21:00 JST on 22 March, when the values of D were small (the mean and the standard deviation: 3.9 ± 2.1~~1–6~~%) compared with those before and after the event, when the values of D were larger than 7.9 ± 2.1~~–8~~% during 15:00 JST on 21 through 15:00 JST on 23, except 03:00–21:00 JST on 22. The main aerosol component during the event might be ~~may have been~~ submicrometer-sized spherical ~~sulfate~~ particles, because D_p was small (4 ± 2~~1–6~~%), and the wavelength exponent Alp was large (1.3 ± 0.3~~–1.4~~). In contrast, the main aerosol particles before and after the event could ~~were assumed to~~ be supermicrometer-sized, nonspherical mineral dust particles because D_p was comparatively large (13 ± 3~~–13~~%) and Alp was ~~approximately 1.0~~ ± 0.2 (Sakai et al., 2003; Cattrall et al., 2005) ~~1.0~~. When there were no clouds above, R at 1064 nm was estimated assuming Alp=1.5 at the reference altitude where very small amount of aerosols was expected to be present, i.e., R=1.06 ± 0.06 (D=1.2 ± 0.51) at 532 nm, in the altitude range 3–6 km. When the value of Alp was changed from 1.0 to 2.0 at the reference altitude, the uncertainty in Alp was estimated to be ± 0.2. The maximum errors of D and D_p were 0.1% and 2% for R>2 at 532 nm.

Line 169 Instead of looking at the variability of depolarization and wavelength exponent between the high aerosol event with the cleaner atmosphere before and after, it is probably more relevant to compare the different aerosol plumes between each other (e.g. March 22 with March 30)

We denoted the variability of Dp and Alp for the two events as follows:

Lines 257-258:

"D_p was small (4 ± 2~~1–6~~%), and the wavelength exponent Alp was large (1.3 ± 0.3~~–1.4~~)" for altitudes of 1.5 km for 03:00–21:00 JST on 22 March.

Line: 355:

"D_p is high (17 ± 6%) for 1–3 km" on 30 March

Line 173 Provide references when interpreting the variability of Dp and Alp.

We provided two references of Sakai et al. (2003) and Cattrall et al. (2005) in line 258.

Section 4

Line 204 Is 225 m the lowest lidar measurement ? See my previous comments. It is important to be clear about this when discussing exchanges between the PBL and the layers aloft.

We added the following sentence in lines 124-125.

The lowest altitude of Mie lidar measurement was 225 m due to the non-perfect overlap of the transmitter-receiver optical axes of the lidar system.

Line 214 There are many possible error sources in aerosol models. A better discussion is needed here including the existing literature about aerosol model errors and specific error quantification of MASINGAR-mk2 which have been already published. It seems that dust concentration is overestimated while pollution aerosol concentration is underestimated when looking at the March 22 and 30 extinction.

We added the following sentences in lines 319-332

The other plausible reason for the underestimation is the uncertainty~~inadequacies~~ of the ~~input anthropogenic~~ emissions inventories of aerosol precursors. Grainer et al.(2011) collected various emission inventories and compared them in global scales. They found that differences in Chinese sulfur dioxide (SO_2) emissions in 2000 reached 66% between the lowest and highest emissions and concluded that there was no consensus among the different inventories for the emissions of Chinese SO_2. This large variation among the inventories indicates that estimate of SO_2 emission in China has large error. In their comparison, the MACCity emission which was used in MASINGAR-mk2 simulation, showed the lower amount of Chinese SO_2 emission among the inventories. This fact might be responsible for the underestimation of pollution aerosol (sulfate) concentrations. In MASINGAR-mk2, dust emission flux is estimated by a parameterized dust emission scheme and has strong dependency upon various parameters (i.e., soil texture, soil wetness, land use, snow cover fraction, vegetation cover, surface wind speed, etc.). The dust model intercomparison project (DMIP; Uno et al., 2006) reported that simulated dust emission amounts over East Asia among eight dust models (including the former version of MASINGAR) differed sometimes by a factor of ten. These facts indicate that estimate of dust emission also causes large errors.

Section 5

Line 240-241 I fully agree with this statement but it is not really developped in the paper.

We discussed on this matter in lines 383-400:

To investigate the vertical transport processes of the aerosol and ozone in the lower troposphere over the measurement site, we show in Figure 11 the time variations of the top altitudes of the atmospheric boundary layers from 11:10 JST on 20 March to 14:33 JST on 31 March 2015 which were estimated from the 1064 nm range-corrected backscatter signals with a range resolution of 15 m using the wavelet covariance transform method (Baars et al., 2008; Izumi et al., 2016), and those obtained from the radiosonde data at Fukuoka and the JMA Meso-scale Analysis (MA) data over Saga using the parcel method (Holzworth, 1964). When the mixed layers developed in the afternoon, the tops of the mixed layers (1.5–2 km) estimated by Mie lidar were almost consistent with those by MA. However, Mie lidar had a tendency to detect the residual layers in the night and morning time, e.g., 21–22 March although the radiosonde data at 9:00 JST on 22 March found the top of the mixed layer was 117 m (Stull, 1988), and it was difficult for Mie lidar to detect the stable boundary layer because the lowest altitude of the Mie lidar measurement was 225 m.

The dust particles originated from the Gobi Desert arrived at 1–3 km altitudes above the residual layer over the lidar site at 06:00 JST on 22 March. When the mixed layer developed to 1.5–2 km at 11:00–15:00 JST on 22, the dust particles were supposed to be mixed into the boundary layer and then

reached the surface by the entrainment, as simulated in Fig.7b. This could result in the sharp increase in PM2.5 concentrations at the surface increased sharply after 11:00 JST, as shown in Fig.4. The similar phenomenon was observed over the northern Kyushu area during the dust event in late May–early June 2014 (Uno et al., 2016).

lines 415-418:

Based on these lidar data, ~~and~~ the in-situ measurement data and the model simulation by MASINGAR -mk2 at Takagimachi in Saga city, there is a possibility that the air mass with high ozone and aerosol concentrations could have been transported from the lower~~free~~ troposphere to the surface by vertical mixing when the planetary boundary layer developed in the afternoon~~daytime~~ of 22 March 2015.

Lidar detection of high concentrations of ozone and aerosol transported from Northeast Asia over Saga, Japan

Osamu Uchino[1, 2], Tetsu Sakai[2], Toshiharu Izumi[2], Tomohiro Nagai[2], Isamu Morino[1], Akihiro Yamazaki[2], Makoto Deushi[3], Keiya Yumimoto[2], Takashi Maki[2], Taichu Y. Tanaka[2], Taiga Akaho[4], Hiroshi Okumura[4], Kohei Arai[4], Takahiro Nakatsuru[1], Tsuneo Matsunaga[1], Tatsuya Yokota[1]

[1]National Institute for Environmental Studies, 16-2 Onogawa, Tsukuba, Ibaraki 305-8506, Japan
[2]Meteorological Research Institute, 1-1 Nagamine, Tsukuba, Ibaraki 305-0052, Japan
[3]Japan Meteorological Agency, 1-3-4 Otemachi, Chiyoda-ku, Tokyo 100-8122, Japan
[4]Saga University, 1 Honjou, Saga, Saga 840-8502, Japan

Correspondence to: O. Uchino (uchino.osamu@nies.go.jp)

Abstract. To validate products of the Greenhouse gases Observing SATellite (GOSAT), we observed vertical profiles of aerosols, thin cirrus clouds, and tropospheric ozone with a mobile lidar system that consisted of a two-wavelength (532 and 1064 nm) polarization lidar and a tropospheric ozone Differential Absorption Lidar (DIAL). We used these lidars to make continuous measurements over Saga (33.24°N, 130.29°E) during 20–31 March 2015. High ozone and high aerosol concentrations were observed almost simultaneously in the altitude range 0.5–1.5 km from 03:00 to 20:00 Japan Standard Time on 22 March 2015. The maximum ozone volume mixing ratio was ~110 ppbv. The maxima of the aerosol extinction coefficient and optical depth at 532 nm were 1.2 km^{-1} and 2.1, respectively. Backward trajectory analysis and the simulations by the Model of Aerosol Species IN the Global AtmospheRe (MASINGAR) mk-2 and the Meteorological Research Institute Chemistry-Climate Model, version 2 (MRI-CCM2) indicated that mineral dust particles originated from the Gobi Desert and an air mass with high ozone and aerosol (mainly sulfate) concentrations ~~could have been transported~~ originated from the North China Plain could have been transported over the measurement site ~~Northeast Asia~~ within about two days. ~~Based on the lidar data and the ground-based in situ measurements at Saga, this air mass could have been transported to the surface by vertical mixing when the planetary boundary layer developed in the daytime~~. These~~is plume, which contained~~ high ozone and aerosol ~~pollutant~~ concentrations~~,~~ impacted surface air quality substantially in the afternoon of 22 March 2015. After some modifications of its physical and chemical parameters, ~~the Meteorological Research Institute Chemistry Climate Model, version 2 (~~MRI-CCM2~~)~~ approximately reproduced the high-ozone volume-mixing ratio. ~~The Model of Aerosol Species IN the Global AtmospheRe (~~MASINGAR~~)~~ mk-2 successfully predicted high aerosol concentrations, but the

predicted peak aerosol optical thickness was about one-third of the observed value.

1 Introduction

Tropospheric ozone is a major air pollutant and impacts human health and vegetation (HTAP, 2010; Yue and Unger, 2014). It is also an important greenhouse gas (IPCC, 2013). Tropospheric aerosols are also air pollutants and aggravate respiratory conditions (HTAP, 2010). Tropospheric aerosols also enhance radiative forcing in a negative (sulfuric acid particles) or positive (black carbon) way (IPCC, 2013), and they affect remote sensing such as the measurement of greenhouse gases from space (Houweling et al., 2005; Uchino et al., 2012a). It is therefore very important to monitor tropospheric ozone and aerosols and to understand their temporal and spatial variations.

To validate products of the Greenhouse gases Observing SATellite (GOSAT), we developed a two-wavelength (532 and 1064 nm) polarization lidar (hereafter abbreviated as Mie lidar) to observe vertical profiles of tropospheric and stratospheric aerosols and thin cirrus clouds at the National Institute for Environmental Studies (NIES), Tsukuba (36.05°N, 140.13°E), Japan in 2009. In 2010 we also developed a DIfferential Absorption Lidar (DIAL) to measure tropospheric ozone profiles (hereafter abbreviated as ozone DIAL). The ozone DIAL was installed in a container with the Mie lidar. In March 2011, we moved the lidar container to Saga (33.24°N, 130.29°E) in the Kyushu district of western Japan at a location 2.6 m above sea level. The ozone DIAL was modified in September 2012 (Uchino et al., 2014).

Mie lidar has been used to demonstrate the influence of high-altitude aerosols and cirrus clouds on the GOSAT product of the column-averaged dry air mole fraction of carbon dioxide (XCO_2) retrieved from the Thermal And Near infrared Sensor for carbon Observation-Fourier Transform Spectrometer (TANSO-FTS) Short-Wavelength InfraRed (SWIR) spectral data onboard GOSAT. The XCO_2 data were improved by taking the vertical profiles of aerosols and cirrus clouds measured by Mie lidar into account (Uchino et al., 2012a). The increases of stratospheric aerosols caused by the 2009 Sarychev eruption and the 2011 Nabro eruption were observed by Mie lidar (Uchino et al., 2012b).

Ozone DIAL has been used to validate the GOSAT ozone product retrieved from TANSO-FTS Thermal InfraRed (TIR) spectral data (Ohyama et al., 2012), to observe ozone concentrations in the lower troposphere, and to compare the observed concentrations with those predicted by the Meteorological Research Institute Chemistry-Climate Model, version 2 (MRI-CCM2) (Deushi and Shibata, 2011). Use of Mie lidar and ozone DIAL will facilitate satellite product validation not only for GOSAT but also for upcoming satellites such as the TROPOspheric Monitoring Instrument (TROPOMI, Veefkind et al., 2012) and the Geostationary Environment Monitoring Spectroscopy (GEMS, Bak et al., 2013). High ozone episodes in the lower troposphere have been observed by lidar (Banta et al., 1998; Koutidis et., 2002; Ancellet et al., 2005; Eisele and Trickl, 2005; Kuang et al., 2011). These observation records were limited to one week at most. We made an 11-day continuous record on 20–31 March 2015.

In this paper we report an event during which high concentrations of ozone and aerosols were observed almost simultaneously below an altitude of 1.5 km over Saga on 22 March 2015, which substantially

impacted surface air quality. We also compared the observational results with those simulated by the models.

2 Characteristics of l~~L~~idar system and observations~~s~~ parameters

Mie lidar and ozone DIAL were installed in a container with dimensions of about 228 cm (width), 683 cm (length), and 255 cm (height), as shown in Fig. 1. Mie lidar is a two-wavelength (532 and 1064 nm) polarization lidar based on a neodymium-doped yttrium-aluminum-garnet (Nd:YAG) laser; the characteristics are summarized in Table 1. The output energy at 532 and 1064 nm was 130 mJ, with a pulse repetition rate of 10 Hz. The diameter of the receiving telescope was 30.5 cm. The output signals from the photomultiplier tubes (PMT) and a silicon avalanche photodiode (APD) were processed by transient recorders with a 12-bit analog/digital converter and a photon counter.

The data analysis methods of Mie lidar and ozone DIAL have been described by Uchino et al. (2012b) and Uchino et al. (2014), respectively. We summarize the observation ~~physical~~ parameters obtained by Mie lidar. The backscattering ratio R is defined as

$$R = (BR + BA)/BR, \quad (1)$$

where BR and BA are the Rayleigh and Mie backscattering coefficients, respectively. Backscattering ratio profiles were derived by the inversion method (Fernald, 1984). The reference altitude was usually set between 9 and 12 km where only molecular backscattering could be assumed when there were no clouds. We assumed the lidar ratio LR~~S~~ (extinction-to-backscatter ratio) for aerosols to be 50 sr at 532 nm and 45 sr at 1064 nm based on the lidar ratios for Asian dust and pollution aerosols summarized by ~~(~~Sakai et al.~~,~~ (2003), Anderson et al. (2003)~~;~~ and Cattrall et al.~~,~~ (2005). To calculate BR, we used the atmospheric molecular density profiles obtained by operational radiosondes at the Fukuoka District Meteorological Observatory (33.58°N, 130.38°E), Japan Meteorological Agency (JMA). The aerosol extinction coefficient was calculated by multiplying BA by S.

The total volume depolarization ratio D was defined as

$$D = S / (P + S) \cdot 100\ (\%), \quad (2)$$

where P and S are the parallel and perpendicular components of the backscattered signals, respectively. The particle depolarization ratio D_p was obtained from the equation

$$D_p = (D \cdot R - D_m)/(R - 1), \quad (3)$$

where D_m is the atmospheric molecular depolarization ratio. We used a D_m value of 0.37% for this lidar

system; we calculated D_m from the spectral transmission data of the interference filter at 532 nm and the Rayleigh backscattering cross sections (Sakai et al., 2003). The value of D_p indicates whether the particles are spherical or non-spherical; large values indicate the presence of non-spherical particles. The backscatter-related Ångström ~~wavelength~~ exponent *Alp*, the qualitative indicator of aerosol particle size ~~shows whether small or large particles account for most of the Mie particles~~, ~~and~~ is defined by

$$BA(\lambda) \propto \lambda^{-Alp}, \quad (4)$$

where λ is the wavelength. Larger values of *Alp* indicate the predominance of smaller (i.e., submicrometer-sized) particles. The vertical resolution of these observation parameters was 150 m, and the time resolution was set to be 1 h for comparison with the Model of Aerosol Species in the Global Atmosphere (MASINGAR)-mk2 (Yukimoto et al., 2012). The lowest altitude of Mie lidar measurement was 225 m due to the non-perfect overlap of the transmitter-receiver optical axes of the lidar system.

The ozone DIAL consisted of a Nd:YAG laser and a 2-m-long Raman cell filled with CO_2 gas that generated four Stokes lines from stimulated Raman scattering by CO_2 ; the characteristics are summarized in Table 2. In this study, we used three Stokes lines (276, 287, and 299 nm). The output energies of these Stokes lines were about 8–9 mJ per pulse, with a pulse repetition rate of 10 Hz. The receiving telescope diameters were 10 cm for boundary layer ozone measurements and 49 cm for free tropospheric ozone measurements. ~~The output signals from the PMTs were also processed by transient recorders with a 12-bit analog/digital converter and a photon counter.~~ ~~The data analysis methods of Mie lidar and ozone DIAL have been described by Uchino et al. (2012b) and Uchino et al. (2014), respectively.~~ The Mie lidar and ozone DIAL were synchronized by two pulse-delay generators.

The 276/287 nm and 287/299 nm wavelength pairs were used for ozone DIAL measurements in the altitude ranges of 0.57–2.0 km and 2.0–6.0 km, respectively. The effective vertical resolutions were 270 m for 0.57–2.0 km and 540 m for 2.0–6.0 km, respectively (Uchino et al., 2014). The time resolution was set to 1 h to facilitate comparison with the MRI-CCM2. The aerosol correction was not made for the ozone retrieval. Next, we report the continuous lidar observational results made at Saga from 20 March to 31 March 2015.

3 Ozone DIAL data

Figure 2a shows a time-altitude cross-section of ozone volume mixing ratios observed by DIAL at Saga from 11:10 JST on 20 March to 14:33 JST on 31 March 2015. Lidar observations were not obtained from 15:56 JST on 27 March to 21:58 JST on 29 March 2015, mainly because of rainy or cloudy ~~bad weather~~ conditions. ~~The vertical resolution was 270 m between altitudes of 450 m and 2 km and 540 m between altitudes of 2 and 6 km. The time resolution was set to 1 h to facilitate comparison with the MRI-CCM2.~~ We made quality checks of the DIAL data. The gray regions in Fig. 2a correspond to areas where there

were no observational data or the errors were larger than 10%. The errors were computed from~~equated to 100% times~~ the lidar signal-to-noise ratios by use of Poisson statistics. Regions surrounded by a black rectangle are areas where the data were affected by aerosols and/or clouds with *R* larger than 2 at 299 nm, which were calculated assuming *LR*=50 sr without correcting attenuation by ozone absorption. In the lowest row of Fig. 2a, we show hourly data of surface oxidant volume mixing ratios (Ox) at Takagimachi in Saga city measured by the Saga Prefectural Environmental Research Center (https://www.pref.saga.lg.jp/web/at-contents/kankyo1/shisetsu/_40810/_41304/_67819.html). Takagimachi is located about 2.8 km northeast from the ozone DIAL site. Because the contribution of other components such as peroxyacetyle nitrate (PAN) to oxidant concentrations was extremely low, the oxidant volume mixing ratio was considered to be that of ozone.

Figure 2a indicates that the ozone volume mixing ratios measured by DIAL were usually about 50–70 ppbv during the study period. Comparatively high ozone concentrations, >75 ppbv, were detected at altitudes of 0.57~~5~~–3 and 0.57~~5~~–2 km on 20–23 March and 30–31 March, respectively. Notably high ozone volume mixing ratios of 90–110 ppbv at altitudes of 0. 57~~5~~–1.5 km were observed from 03:00 to 20:00 JST on 22 March. These high ozone concentrations were also seen in the surface photochemical oxidants data, i.e., the Ox equaled 92–101 ppbv from 15:00 to 21:00 JST on 22 March, as shown in the lowest row in Fig. 2a. The maximum concentration of Ox was 101 ppbv at 16:00 JST. This maximum value was far above the environmental quality standard of 60 ppbv for hourly photochemical oxidants in Japan (https://www.env.go.jp/en/air/aq/aq.html). ~~These observational results show the descent of regions of high ozone concentrations and suggest that air with high ozone concentrations was transported to the surface by vertical mixing when the planetary boundary layer developed during the daytime.~~

3.1 Comparison of DIAL data with MRI CCM-2

The MRI-CCM2 is a global model that simulates chemical and physical processes that affect the distribution and evolution of ozone and other trace gases from the surface to the stratosphere (Deushi and Shibata, 2011). Uchino et al. (2014) have provided an outline of MRI-CCM2. The vertical resolution of the model increases from about 100 to 600 m from the surface to 6 km. The time step of the transport (chemistry) scheme is 30 (15) min. We used hourly model output data. The horizontal resolution is about 110 km. We examined whether or not the model could simulate DIAL observational results. The MRI-CCM2 simulated the DIAL observations reasonably well. However, the MRI-CCM2 predicted the high ozone concentrations of 50–60 ppbv and could not reproduce those ~~the high ozone concentrations~~ of 90–110 ppbv observed with DIAL below an altitude of 1.5 km during 03:00–20:00 JST on 22 March 2015. We therefore performed some simulations in which we changed the emission inventory data and the term that forced the reanalysis wind field. The most reasonable results which were shown in Fig.2b were obtained when the following changes were made ~~(Fig. 2b)~~. The e-folding time of the nudging term was changed from 18 hours to 12 hours to more strongly force the simulated wind fields toward the reanalysis data. In addition, we changed the emission inventory of Regional Emission inventory in Asia version 1.1

(REAS 1.1) (Ohara et al., 2007) to REAS 2.1 (Kurokawa et al., 2013) and the NO_2/NO_x emissions ratio from 5% to 15% by volume, which is within the range of uncertainty (Carslaw, 2005). The emission inventory of NO_x increased about 50% from REAS 1.1 to REAS 2.1. Figure 2c shows the differences between the observed and simulated ozone mixing ratios. Simulated ozone volume mixing ratios were about 60–70 ppbv below an altitude of 1.5 km from 14:00 JST on 21 March to 21:00 JST on 22 March 2015, lower by about 20–50 ppbv compared with the DIAL results. And the MRI-CCM2 predicted the high ozone concentration a half day earlier than the DIAL observation.

The maximum bias (systematic error) of ozone DIAL data caused by aerosols was estimated to be 20% (15 ppbv) at 0.57 km, and the mean bias and the standard deviation were 7% ± 5% in the altitude range 0.57–2.0 km at 11:00 JST. These biases were estimated from *Alp* observed at the same time by Mie lidar and assuming *LR* =50 sr in the wavelength range 276–299 nm, based on the equations of (6) and (7) in Uchino and Tabata (1991). These biases were not large since the 276/287 nm and 287/299 nm wavelength pairs were suitable for measurements of ozone in the boundary layer and the free troposphere respectively (Nakazato et al., 2007). As mentioned earlier, the ozone DIAL data with the statistical error smaller than 10% was used in this study. Therefore the uncertainty of the ozone DIAL data was estimated to be smaller than 22% and the mean value of the uncertainty was 12%. A model with higher horizontal resolution might be necessary to more realistically simulate high surface ozone concentration events in the planetary boundary layer.

4 Mie lidar data

~~First, we summarize the physical parameters obtained by Mie lidar. The backscattering ratio *R* is defined as~~

~~$R = (BR + BA)/BR,$ (1)~~

~~where *BR* and *BA* are the Rayleigh and Mie backscattering coefficients, respectively. Backscattering ratio profiles were derived by the inversion method (Fernald, 1984). We assumed the lidar ratio *LRS* (extinction to backscatter ratio) for aerosols to be 50 sr at 532 nm and 45 sr at 1064 nm (Sakai et al., 2003; Cattrall et al., 2005). To calculate *BR*, we used the atmospheric molecular density profiles obtained by operational radiosondes at the Fukuoka District Meteorological Observatory (33.58°N, 130.38°E), Japan Meteorological Agency (JMA). The aerosol extinction coefficient was calculated by multiplying *BA* by *S*.~~

~~The total volume depolarization ratio *D* was defined as~~

~~$D = S / (P + S) \cdot 100\ (\%),$ (2)~~

where P and S are the parallel and perpendicular components of the backscattered signals, respectively. The particle depolarization ratio D_p was obtained from the equation

$$D_p = (D \cdot R - D_m)/(R - 1), \quad (3)$$

where D_m is the atmospheric molecular depolarization ratio. We used a D_m value of 0.37% for this lidar system; we calculated D_m from the spectral transmission data of the interference filter at 532 nm and the Rayleigh backscattering cross sections (Sakai et al., 2003). The value of D_p indicates whether the particles are spherical or non spherical; large values indicate the presence of non spherical particles. The wavelength exponent, *Alp*, shows whether small or large particles account for most of the Mie particles and is defined by

$$BA(\lambda) \propto \lambda^{-Alp}, \quad (4)$$

where λ is the wavelength. Larger values of *Alp* indicate the predominance of smaller (i.e., submicrometer-sized) particles.

Figures 3a, and 3b, and 3c show time-altitude cross-sections of the backscattering ratio (R), and the total volume depolarization ratio (D), and the particle depolarization ratio (D_p), respectively, observed by Mie lidar at Saga from 11:10 JST on 20 March to 14:33 JST on 31 March 2015. Mie lidar data observation were not obtained from 15:56 JST on 27 March to 21:58 JST on 29 March 2015, mainly because of rainy and very low cloudbad weather conditions. The vertical resolution was 150 m, and the time resolution was set to be 1 h for comparison with the Model of Aerosol Species in the Global Atmosphere (MASINGAR) mk2 (Yukimoto et al., 2012). We made quality checks of Mie lidar data. Gray regions are areas where there were no observational data or the data were affected by clouds.

Aerosol layers with R in the range 2–4 almost always existed below an altitude of 2.5 km for 20–31 March 2015. An event of high aerosol loading with large values of R (>8~~4–19~~) was observed below altitudes of 1.5 km for 03:00–21:00 JST on 22 March, when the values of D were small (the mean and the standard deviation: 3.9 ± 2.1~~1–6~~%) compared with those before and after the event, when the values of D were larger than 7.9 ± 2.1~~–8~~% during 15:00 JST on 21 through 15:00 JST on 23, except for 03:00–21:00 JST on 22. The main aerosol component during the event might be ~~may have been~~ submicrometer-sized spherical ~~sulfate~~ particles, because D_p was small (4 ± 2~~1–6~~%), and the wavelength exponent *Alp* was large (1.3 ± 0.3~~–1.4~~). In contrast, the main aerosol particles before and after the event could ~~were assumed to~~ be supermicrometer-sized, nonspherical mineral dust particles because D_p was comparatively large (13 ± 3~~–13~~%) and *Alp* was ~~approximately~~ 1.0 ± 0.2 (Sakai et al., 2003; Cattrall et al., 2005) ~~1.0~~. When there were no clouds above, R at 1064 nm was estimated assuming *Alp*=1.5 at the reference altitude where very small amount of aerosols was expected to be present, i.e., R=1.06 ± 0.06 (D=1.2 ± 0.5) at 532 nm, in the altitude range 3–6 km. If the value of *Alp* was changed from 1.0 to 2.0 at the reference altitude, the uncertainty in *Alp* was estimated to be ± 0.2. *Alp* was 0.3–2.0 in the 11-day Mie lidar record. The

maximum errors of D and D_p were 0.1% and 2% for R>2 at 532 nm.

During the same time period, high aerosol concentrations were also observed at the surface (Fig.4). Hourly values of the mass concentrations of particulate matter with a diameter of 2.5 μm or less ($PM_{2.5}$) at Takagimachi measured by the Saga Prefectural Environmental Research Center were 23 μg m^{-3} at 10:00 JST and increased up to a maximum value of 110 μg m^{-3} at 15:00 JST on 22 March; the concentrations were greater than 82 μg m^{-3} during 13:00–16:00 JST and decreased to 17 μg m^{-3} at 01:00 JST on 23 March. The daily mean value of $PM_{2.5}$ was 50.6 μg m^{-3} for 24 hours on 22 March at Takagimachi, larger than the environmental quality standard of 35 μg m^{-3} in Japan (https://www.env.go.jp/en/air/aq/aq.html). ~~Consideration of the lidar data and the temporal variation of $PM_{2.5}$ at Takagimachi suggests that air with high concentrations of both aerosols and ozone was transported to the surface by vertical mixing when the planetary boundary layer developed in the daytime~~.

4.1 Comparison of Mie lidar data with MASINGAR mk-2

The MASINGAR-mk2 is an improved version of the MASINGAR aerosol model (Tanaka et al., 2003); it treats five aerosol species: sulfate, black and organic carbon, sea salt, and soil dust. We used emission data for sulfur dioxide and for black and organic carbon from MACCity (Granier et al., 2011). Soil dust and sea salt were represented by 10 bins with particle diameters of 0.2–20 μm. The model was coupled online with the atmospheric general circulation model MRI-AGCM3 (Yukimoto et al., 2012). The Meteorological fields were from JMA Global Analysis data (GANAL). The horizontal resolution of the MASINGAR-mk2 was about 60 km, and the number of vertical layers was 40 from the surface to 0.1 hPa. The vertical resolutions were 100, 300, and 600 m at the lowest level and altitudes of 1 and 6 km, respectively. The time step of the transport (chemistry) scheme was 450 seconds, and we used hourly model output data.

Figures 4a and 4b show the time-height cross sections of aerosol extinction coefficients observed by Mie lidar and simulated by MASINGAR-mk2, respectively. Figure 4c represents the difference between the observed and simulated extinction coefficients. The model was able to capture the general characteristics of the observational results rather well. A close look at Fig. 4c reveals that the model underestimated the aerosol extinction coefficients of the anthropogenic pollutant event on 22 March but slightly overestimated the extinction coefficients associated with particles having larger total volume depolarization ratios on 30 and 31 March (i.e., dust-dominant case).

4.2 Comparison of aerosol optical depths

Figure 5 shows temporal variations of the aerosol optical depths (AOD) measured by Mie lidar at 532 nm and sky radiometer at 500 nm (Kobayashi et al., 2006, Uchino et al., 2012a) and simulated at 550 nm by MASINGAR-mk2 from 20 to 31 March. To estimate AODs from the lidar data, the extinction coefficient at 225 m was extrapolated to the ground, the extinction coefficient from 15 to 35 km was observed at

night on the same day, and *S* was assumed to be 50 sr for all altitudes. When clouds and thick aerosols were present, AODs were not obtained. The sky radiometer was positioned on the roof of the building, which is four stories high and located to the west of the container (brown building in Fig. 1). Although it must be noted that the measured and simulated wavelengths differed slightly, the AODs were almost the same, except for the high aerosol and ozone event on 22 March. The mean bias and the standard deviation of AOD between Mie lidar and sky radiometer was 0.029 ± 0.051, and that between MASINGAR mk-2 and sky radiometer was –0.07 ± 0.24 for 20–31 March, except for 12:00–14:00 JST on 22 March. The maximum values of the AODs were 2.1 at 12:00 JST by lidar, 1.92 at 13:00 JST by sky radiometer, and 0.53 at 13:00 JST by MASINGAR-mk2. One possible reason for the large difference in AOD (~0.2) between Mie lidar and Sky radiometer data is that we set the reference altitudes 8.2 km and 2.8 km at 12:00 and 13:00 JST on 22 March respectively for the lidar because the backscattered signals were strongly attenuated by the dense aerosol layers below 2 km. This might cause error in AODs for the Mie lidar data.

The model underestimated the AODs by factors of about 3.6–4 compared to the sky radiometer and lidar observations. One plausible reason for that is that the model resolution (about 60 km) was insufficient to reproduce the observed prominent peak in which the observed AOD increased from 1.0 to 2.0 in 6 hours. The other plausible reason for the underestimation is the uncertainty ~~inadequacies~~ of the ~~input anthropogenic~~ emissions inventories of aerosol precursors. Grainer et al. (2011) collected various emission inventories and compared them in global scales. They found that differences in Chinese sulfur dioxide (SO_2) emissions in 2000 reached 66% between the lowest and highest emissions and concluded that there was no consensus among the different inventories for the emissions of Chinese SO_2. This large variation among the inventories indicates that estimate of SO_2 emission in China has large error. In their comparison, the MACCity emission which was used in MASINGAR-mk2 simulation, showed the lower amount of Chinese SO_2 emission among the inventories. This might be responsible for the underestimation of pollution aerosol (sulfate) concentrations. In MASINGAR-mk2, dust emission flux is estimated by a parameterized dust emission scheme and has strong dependency upon various parameters (i.e., soil texture, soil wetness, land use, snow cover fraction, vegetation cover, surface wind speed, etc.). The dust model intercomparison project (DMIP; Uno et al., 2006) reported that simulated dust emission amounts over East Asia among eight dust models (including the former version of MASINGAR) differed sometimes by a factor of ten. These facts indicate that estimate of dust emission also causes large errors. To solve this problem, for example, it might be better to use the near real-time satellite data of SO_2~~sulfur dioxide~~ and nitrogen dioxide (NO_2) provided by the Ozone Monitoring Instrument (OMI) onboard NASA's Aura satellite (Krotkov et al., 2016)~~.~~, and/or to use a data assimilation technique that integrates model simulation and observation data (Yumimoto et al., 2016).

5 Discussion: origin and transport pathways of ozone and aerosol plumes ~~and concluding remarks~~

~~By using ozone DIAL and a two-wavelength polarization (Mie) lidar, we made continuous measurements of ozone and aerosol concentrations over Saga during 20–31 March 2015, with the exception of a period with rainy and very low cloudbad weather conditions. High ozone and high aerosol concentrations that occurred nearly simultaneously were observed in the altitude range 0.5–1.5 km from 03:00 to 20:00 JST on 22 March 2015. The ozone volume mixing ratio was larger than 100 ppbv. The aerosol extinction coefficient and AOD at 532 nm were larger than 0.5 km^{-1} and 1.5, respectively.~~

Figure 7 shows the time-altitude cross sections of total aerosol extinction coefficients at 550 nm, and the ratios of dust extinction coefficients to total aerosol extinction coefficients simulated by MASINGAR-mk2 with potential temperatures over Saga for 20–31 March 2015. For the event on 22 March, the model predicted the dust particles (60–100%) in the altitude range 1–3 km, and sulfate (40–60%) and dust (30–40%) particles below 1 km. The number of the parenthesis represents the ratio of each component's extinction coefficient to the total extinction coefficient. The dust particles descended to the surface in the afternoon (Fig.7b). For the event on 30 March, MASINGAR mk-2 predicted the dust particles (50–100%) for 1–6 km, and sulfate (50–80%) and dust (0–20%) particles below 1 km in the morning. Mie lidar data support the model prediction because D_p is high (17 ± 6%) for 1–3 km and low (10 ± 3%) below 1 km. For both events, small amounts of organic carbon, black carbon and sea salt particles were predicted.

To identify the origin of the ~~ozone and~~ aerosols and related transport processes, three-dimensional backward trajectories of air parcels were calculated with the NOAA Hybrid Single Particle Lagrangian Integrated Trajectory (HYSPRIT) model (Draxler and Hess, 1998; Stein et al., 2015)~~, as shown in Fig. 6.~~ An~~Twenty seven~~ air parcel~~s~~ was ~~were~~ initially left at altitudes of ~~600–1000~~ 1500 m (Fig. 8a) and 500 m (Fig.9a) over the lidar site at Saga. The trajectories were calculated for three days from 21~~00~~:00 UTC ~~(09:00 JST)~~ on 21~~2~~ (06:00 JST on 22) March 2015. Figures 8b and 9b show the time-altitude cross sections of dust and sulfate extinction coefficients simulated by MASINGAR mk-2 along the trajectory paths of Figs. 8a and 9a, respectively. Based on the results of the backward trajectories and the model simulations, the dust and sulfate particles ~~high ozone and aerosol concentrations~~ on 22 ~~and 31~~ March could have been transported within about two days from the Gobi Desert and the North China Plain (NCP), respectively, to the measurement site~~the Northeast Asia~~. The highest concentrations of SO_2 and NO_2 in the world were observed in NCP for 2013–2015 by the Ozone Monitoring Instrument (OMI) onboard NASA's Aura satellite, as shown in Fig.5 by Krotkov et al. (2016). These gases are important precursors of sulfate particles and ozone. Figure 10 represents the horizontal maps of ozone volume mixing ratios at 925 hPa (about 760 m altitude) simulated by MRI-CCM2 at 21:00 JST on 19, 20, 21 March and at 03:00 JST on 22 March 2015. These maps indicate that the high ozone could be transported from NCP to the Yellow Sea and then Saga within about two days.

Because it was difficult to obtain observational data of surface ozone and sulfate particles in NCP including Beijing on 19-20 March, we refer to the following papers related to those data. According to the ozonesonde measurements made by Wang et al. (2012), ozone concentrations ≥90 ppbv were observed over Beijing, China in late March. Ma et al. (2016) reported a significant increase of surface ozone from 2003 to 2015 at Shangdianzi (40.65°N, 117.10°E), which is located about 100 km northeast of suburban

Beijing, and the maximum daily average 8-h concentrations of ozone appear to have been >100 ppbv in March 2015 based on Fig. 2 in their paper. High $PM_{2.5}$ and submicron aerosol concentrations have been observed in Beijing (Zhang et al., 2013; Sun et al., 2015). Ozone and aerosol concentrations may therefore have been high in March 2015 over NCP~~Northeast Asia~~.

To investigate the vertical transport processes of the aerosol and ozone in the lower troposphere over the measurement site, we show in Figure 11 the time variations of the top altitudes of the atmospheric boundary layers from 11:10 JST on 20 March to 14:33 JST on 31 March 2015 which were estimated from the 1064 nm range-corrected backscatter signals with a range resolution of 15 m using the wavelet covariance transform method (Baars et al., 2008; Izumi et al., 2016), and those obtained from the radiosonde data at Fukuoka and the JMA Meso-scale Analysis (MA) data over Saga using the parcel method (Holzworth, 1964). When the mixed layers developed in the afternoon, the tops of the mixed layers (1.5–2 km) estimated by Mie lidar were almost consistent with those by MA. However, Mie lidar had a tendency to detect the residual layers in the night and morning time, e.g., 21–22 March. Although the radiosonde data at 9:00 JST on 22 March found the top of the mixed layer was 117 m (Stull, 1988), it was difficult for Mie lidar to detect the mixed layer because the lowest altitude of the Mie lidar measurement was 225 m.

The dust particles originated from the Gobi Desert arrived at 1–3 km altitudes above the residual layer over the lidar site at 06:00 JST on 22 March. When the mixed layer developed to 1.5–2 km at 11:00–15:00 JST on 22, the dust particles were supposed to be mixed into the boundary layer and then reached the surface by the entrainment, as simulated in Fig.7b. This could result in the sharp increase in PM2.5 concentrations at the surface after 11:00 JST, as shown in Fig.4. The similar phenomenon was observed over the northern Kyushu area during the dust event in late May–early June 2014 (Uno et al., 2016). A similar high-surface-ozone event was observed by eight ozonesonde measurements during 6–9 June 2003 over the Seoul metropolitan region (Oh et al., 2010).

6. Concluding remarks

By using ozone DIAL and a two-wavelength polarization (Mie) lidar, we made continuous measurements of ozone and aerosol concentrations over Saga during 20–31 March 2015. High ozone and high aerosol concentrations that occurred nearly simultaneously were observed in the altitude range 0.5–1.5 km from 03:00 to 20:00 JST on 22 March 2015. The ozone volume mixing ratio was larger than 100 ppbv. The aerosol extinction coefficient and AOD at 532 nm were larger than 0.5 km^{-1} and 1.5, respectively.

Backward trajectory analysis and the simulations by the MASINGAR mk-2 and the MRI-CCM2 models indicated that the mineral dust particles originated from the Gobi Desert and an air mass with high ozone and aerosol (mainly sulfate) concentrations originated from the North China Plain could have been transported over the lidar site within about two days. Based on the lidar and surface measurement data and the simulation by MASINGAR-mk2, there is a possibility that the air mass with high ozone and

aerosol concentrations could have been transported from the lower~~free~~ troposphere to the surface by vertical mixing when the planetary boundary layer developed in the afternoon~~daytime~~ of 22 March 2015. The combination of ozone DIAL measurements with surface in-situ ozone measurements is very useful for studying the process of descent of high ozone concentrations in the lower~~free~~ troposphere to the surface and the impacts on surface air quality. Such measurements of pollution plumes that descend from the free troposphere to the surface are highly recommended (HTAP, 2010).

The MRI-CCM2 could approximately reproduce the high-ozone volume-mixing ratios after some modifications of physical and chemical parameters. MASINGAR mk-2 successfully predicted high aerosol concentration events, but the predicted peak AOD was about one-third of the observed AOD. For further improvement of these models, it will be important to continue comparing these models with ozone DIAL, Mie lidar, and surface in-situ ozone and particle measurements.

Acknowledgements. We used radiosonde data measured by the Japan Meteorological Agency and hourly concentrations of surface oxidant and $PM_{2.5}$ measured by the Saga Prefectural Environmental Research Center. The NOAA Hybrid Single Particle Lagrangian Integrated Trajectory (HYSPRIT) model was used to calculate backward trajectories of air parcels.

455 **References**

456 Ancellet, G. and Ravetta, F.: Analysis and validation of ozone variability observed by lidar during the
457 ESCOMPTE-2001 campaign, Atmos. Res., 74, 435-459, 2005.
458 Anderson, T. L., Masonis, S. J., Covert, D. S., Ahlquist, N. C., Howell, S. G., Clarke, A. D., and
459 McNaughton, C. S.: Variability of aerosol optical properties derived from in situ aircraft
460 measurements during ACE-Asia, J. Geophys. Res., 108, D23, 8647, doi:10.1029/2002JD003247, 2003.
461 Baars, H., Ansmann, A., Engelmann, R., and Althausen, D.: Continuous monitoring of the boundary-layer
462 top with lidar, Atmos. Chem. Phys., 8, 7281-7296, 2008.
463 Bak, J., Kim, J. H., Liu, X., Chance, K., and Kim, J.: Evaluation of ozone profile and tropospheric ozone
464 retrievals from GEMS and OMI spectra, Atmos. Meas. Tech., 6, 239-249, doi:10.5194/amt-6-239-
465 2013, 2013.
466 Banta, R. M., Senff, C. J., White, A. B., Trainer, M., McNider, R. T., Valente, R. J., Mayor, S. D., Alvarez,
467 R. J., Hardesty, R. M., Parrish, D., and Fesenfeld, F. C.: Daytime buildup and nighttime transport of
468 urban ozone in the boundary layer during a stagnation episode, J. Geophys. Res., 103, D17, 22519-
469 22544, 1998.
470 Carslaw, D. C.: Evidence of an increasing NO_2/NO_x emissions ratio from road traffic emissions, Atmos.
471 Env., 39, 4793-4802, 2005.
472 Cattrall, C., Reagan, J., Thome, K., and Dubovik, O.: Variability of aerosol and spectral lidar and
473 backscatter and extinction ratios of key aerosol types derived from selected Aerosol Robotic Network
474 locations, J. Geophys. Res., 110, D10S11, doi:10.1029/2004JD005124, 2005.
475 Deushi, M. and Shibata, K.: Development of a Meteorological Research Institute Chemistry-Climate
476 Model version 2 for the study of tropospheric and stratospheric chemistry, Pap. Meteorol. Geophys.,
477 62, 1-46, doi:10.2467/mripapers.62.1, 2011.
478 Draxler, R. R. and Hess, G. D.: An overview of the HYSPLIT_4 modeling system for trajectories,
479 dispersion, and deposition, Aust. Meteor. Mag., 47, 295-308, 1998.
480 Eisele, H. and Trickl, T.: Improvements of the aerosol algorithm in ozone lidar data processing by use of
481 evolutionary strategies, 44, 2638-2651, 2005.
482 Fernald, F. G.: Analysis of atmospheric lidar observations: some comments, Appl. Opt., 23, 652-653,
483 1984.
484 Granier, C., Bessagnet, B., Bond, T., D'Angiola, A., van der Gon, H. D.., Frost, G. J., Heil, A., Kaiser, J.
485 W., Kinne, S., Klimont, Z., Kloster, S., Lamarque, J. -F., Liousse, C., Masui, T., Meleux, F., Mieville,
486 A., Ohara, T., Raut, J.-C., Riahi, K., Schultz, M. G., Smith, S. J., Thompson, A., van Aardenne, J., van
487 der Werf, G. R., and van Vuuren, D. P.: Evolution of anthropogenic and biomass burning emission of
488 air pollutants at global and regional scales during the 1980–2010 period, Clim. Change, 109, 163–190,
489 2011.
490 Hemispheric Transport of Air Pollution (HTAP) 2010, Part A: Ozone and particulate matter, edited by:
491 Dentener, F., Keating, T., and Akimoto, H., Air Pollution Studies No. 17, United Nations, New York
492 and Geneva, 278 pp., 2010.

493 Holzworth, G. C.: Estimates of mean maximum mixing depths in the contiguous United States, Mon.
494 Weather Rev., 92, 235-242, 1964.
495 Houweling, S., Hartmann, W., Aben, I., Schrijver, H., Skidmore, J., Roelofs, G.-J., and Breon, F.-M.:
496 Evidence of systematic errors in SCIAMACHY-observed CO_2 due to aerosols, Atmos. Chem. Phys., 5,
497 3003-3013, 2005.
498 Intergovernmental Panel on Climate Change (IPCC): Climate Change 2013: The Physical Science Basis:
499 Contribution of Working Group I to the Fifth Assessment Report of the Intergovernmental Panel on
500 Climate Change, edited by: Stocker, T.F., Qin, D., Plattner, G.-K., Tignor, M., Allen, S.K., Boschung,
501 J., Nauels, A., Xia, Y., Bex, V., and Midgley, P.M., Cambridge University Press, Cambridge, United
502 Kingdom and New York, NY, USA, 1535 pp, doi:10.1017/CBO9781107415324, 2013.
503 Izumi, T., Uchino, O., Sakai, T., Nagai, T., and Morino, I.: Mixed layer height calculated from Mie lidar
504 data, submitted to Tenki, 2016 (in Japanese).
505 Kobayashi, E., Uchiyama, A., Yamazaki, A., and Matsuse, K: Application of the maximum likelihood
506 method to the inversion algorithm for analyzing aerosol optical properties from sun and sky radiance
507 measurements, J. Meteor. Soc. Jpn., 84, 1047-1062, 2006.
508 Kourtidis, K., Zerefos, C., Rapsomanikis, S., Simeonov, V., Balis, D., Perros, P. E., Thompson, A. M.,
509 Witte, J., Calpini, B., Sharobiem, W. M., Papayannis, A., Mihalopoulos, N., and Drakou, R.: Regional
510 levels of ozone in the troposphere over eastern Mediterranean, J. Geophys. Res., 107, D18, 8140,
511 doi:10.1029/2000JD000140, 2002.
512 Krotkov, N. A., McLinden, C. A., Li, C., Lamsal, L. N., Celarier, E. A., Marchenko, S. V., Swartz, W. H.,
513 Bucsela, E. J., Joiner, J., Duncan, B. N., Boersma, K. F., Veefkind, J. P., Levelt, P. F., Fioletov, V. E.,
514 Dickerson, R. R., He, H., Lu, Z., and Streets, D. G.: Aura OMI observations of regional SO_2 and NO_2
515 pollution changes from 2005 to 2015, Atmos. Chem. Phys., 16, 4605-4629, doi:10.5194/acp-16-4605-
516 2016, 2016.
517 Kuang, S., Newchurch, M. J., Burris, J., Wang, L., Buckley, P. I., Johnson, S., Knupp, K., Huang, G.,
518 Phillips, D., and Cantrell, W.: Nocturnal ozone enhancement in the lower troposphere observed lidar,
519 Atmos. Environ., 45, 6078-6084, 2011.
520 Kurokawa, J., Ohara, T., Morikawa, T., Hanayama, S., Janssens-Maenhout, G., Fukui, T., Kawashima,
521 K., and Akimoto, H.: Emissions of air pollutants and greenhouse gases over Asian regions during
522 2000–2008: Regional Emission inventory in ASia (REAS) version 2, Atmos. Chem. Phys., 13, 11019–
523 11058, doi: 10.5194/acp-13-11019-2013, 2013.
524 Ma, Z., Xu, J., Quan, W., Zhang, Z., Lin, W., and Xu, X.: Significant increase of surface ozone at a rual
525 site, north of eastern China, Atmos. Chem. Phys., 16, 3969-3977, doi:10.5194/acp-16-3969-2016,
526 2016.
527 Nakazato, M., Nagai, T., Sakai, T., and Hirose, Y.: Tropospheric ozone differential-absorption lidar using
528 stimulated Raman scattering in carbon dioxide, Apl. Opt., 46, 2269-2279, 2007.
529 Oh, I.-B., Kim, Y.-K., Hwang, M.-K., Kim, C.-H., Kim, S., and Song, S.-K.: Elevated ozone layers over
530 the Seoul metropolitan region in Korea: evidence for long-range ozone transport from eastern China

and its contribution to surface concentrations, J. Appl. Meteor. and Climat., 49, 203-220, doi:10.1175/2009JAMC2213.1, 2010.

Ohara, T., Akimoto, H., Kurokawa, J., Horii, N., Yamaji, K., Yan, X., and Hayasaka, T.: An Asian emission inventory of anthropogenic emission sources for the period 1980-2020, Atmos. Chem. Phys., 7, 4419-4444, doi:10.5194/acp-7-4419-2007, 2007.

Ohyama, H., Kawakami, S., Shiomi, K., and Miyagawa, K.: Retrievals of total and tropospheric ozone from GOSAT thermal infrared spectral radiances, IEEE Trans. Geosci. Remote Sens., 50, 1770-1784, doi:10.1109/TGRS.2001.2170178, 2012.

Sakai, T., Nagai, T., Nakazato, M., Mano, Y., and Matsumura, T.: Ice clouds and Asian dust studied with lidar measurements of particle extinction-to-backscatter ratio, particle depolarization, and water-vapor mixing ratio over Tsukuba, Appl. Opt., 42, 7103-7116, 2003.

Stein, A. F., Draxler, R. R., Rolph, G. D., Stunder, B. J. B., Cohen, M. D., and Ngan, F.: NOAA's HYSPLIT atmospheric transport and dispersion modeling system, Bull. Amer. Meteor. Soc., 96, 2059-2077, 2015.

Stull, R. B.: An introduction to boundary layer meteorology, Klumer Academic Publications, 670 pp, 1988.

Sun, Y. L., Wang, Z. F., Du, W., Zhang, Q., Wang, Q. Q., Fu, P. Q., Pan, X. L., Li, J., Jayne, J., and Worsnop, D. R.: Long-term real-time measurements of aerosol particle composition in Beijing, China: seasonal variations, meteorological effects, and source analysis, Atmos. Chem. Phys., 15, 10149-10165, doi:10.5194/acp-15-10149-2015, 2015.

Tanaka, T. Y., Orito, K., T. T. Sekiyama, Shibata, K., Chiba, M., and Tanaka, H.: MASINGAR, a global tropospheric aerosol chemical transport model coupled with MRI/JMA98 GCM: Model description, Pap. Meteor. Geophys., 53(4), 119-138, 2003.

Uchino, O. and Tabata, I.: Mobile lidar for simultaneous measurements of ozone, aerosols, and temperature in the stratosphere, Appl. Opt., 30, 2005-2012, 1991.

Uchino, O., Kikuchi, N., Sakai, T., Morino, I., Yoshida Y., Nagai, T., Shimizu, A., Shibata, T., Yamazaki, A., Uchiyama, A., Kikuchi, N., Oshchepkov, S., Brill, A., and Yokota, T., Influence of aerosols and thin cirrus clouds on the GOSAT-observed CO_2: a case study over Tsukuba, Atmos. Chem. Phys., 12, 3393–3404, doi:10.5194/acp-12-3393-2012, 2012a.

Uchino, O., Sakai, T., Nagai, T., Nakamae, K., Morino, I., Arai, K., Okumura, H., Takubo, S., Kawasaki, T., Mano, Y., Matsunaga, T., and Yokota, T., On recent (2008–2012) stratospheric aerosols observed by lidar over Japan, Atmos. Chem. Phys., 12, 11975–11984, doi:10.5194/acp-12-11975-2012, 2012b.

Uchino, O., Sakai, T., Nagai, T., Morino, I., Maki, T., Deushi, M., Shibata, K., Kajino, M., Kawasaki, T., Akaho, T., Takubo, S., Okumura, H., Arai, K., Nakazato, M., Matsunaga, T., Yokota, T., Kawakami, S., Kita, K., and Sasano, Y.: DIAL measurement of lower tropospheric ozone over Saga (33.24°N, 130.29°E) , Japan, and comparison with a chemistry–climate model, Atmos. Meas. Tech., 7, 1385-1394, doi:10.5194/amt-7-1385-2014, 2014.

Uno, I., Wang, Z., Chiba, M., Chun, Y. S., Gong, S. L., Hara, Y., Jung, E., Lee, S.-S., Liu, M., Mikami,

M., Music, S., Nickovic, S., Satake, S., Shao, Y., Song, Z., Sugimoto, N., Tanaka, T., and Westphal, D. L.: Dust model intercomparison (DMIP) study over Asia: Overview, J. Geophys. Res., 111, D12213, doi:10.1029/2005JD006575, 2006.

Uno, I., Pan, X., Itahashi, S., Yumimoto, K., Hara, Y., Kuribayashi, M., Yamamoto, S., Shimohara, T., Tamura, K., Ogata, Y., Osada, K., Kamikuchi, Y., Yamada, S., and Kobayashi, H.: Overview of long-range yellow sand and high concentration of air pollution observed over the northern Kyusyu area in late May-early June 2014, J. Jpn. Soc. Atmos. Environ., 51, 44-57, 2016.

Veefkind, J. P., Aben, I., McMullan, K., Förster, H., de Vries, J., Otter, G., Claas, J., Eskes, H. J., de Haan, J. F., Kleipool, Q., van Weele, M., Hasekamp, O., Hoogeveen, R., Landgraf, J., Snel, R., Tol, P., Ingmann, P., Voors, R., Kruizinga, B., Vink, R., Visser, H., and Levelt, P. F.: TROPOMI on the ESA Sentinel-5 Precursor: A GMES mission for global observations of the atmospheric composition for climate, air quality and ozone layer applications, Remote Sens. Environ., 120, 70-83, 2012.

Wang, Y., Konopka, P., Liu, Y., Che, H., Müller, R., Plöger, F., Riese, M., Cai, Z., and Lü, D.: Tropospheric ozone trend over Beijing from 2002-2010: ozonesonde measurements and modeling analysis, Atmos. Chem. Phys., 12, 8389-8399, doi:10.5194/acp-12-8389-2012, 2012.

Yue, X. and Unger, N., Ozone vegetation damage effects on gross primary productivity in the United States, Atmos. Chem. Phys., 14, 9137-9153, doi:10.5194/acp-14-9137-2014, 2014.

Yukimoto, S., Adachi, Y., Hosaka, M., Sakami, T., Yoshimura, H., Hirabara, M., Tanaka, T. Y., Shindo, E., Tsujino, H., Deushi, M., Mizuta, R., Yabu, S., Obata, A., Nakano, H., Koshiro, T., Ose, T., and Kitoh, A.: A new global climate model of the Meteorological Research Institute: MRI-CGCM3 —Model Description and Basic Performance—, J. Meterol. Soc. Jpn., 90A, 23-64, doi:10.2151/jmsj.2012-A02. 2012.

Yumimoto, K., Nagao, T. M., Kikuchi, M., Sekiyama, T. T., Murakami, H., Tanaka, T. Y., Ogi, A., Irie, H., Khatari, P., Okumura, H., Arai, K., Morino, I., Uchino, O., and Maki, T.: Aerosol data assimilation using data from Himawari-8, a next-generation geostationary meteorological satellite, Geophys. Res. Lett., 43, doi:10.1002/2016GL069298.

Zhang, R., Jing, J., Tao, J., Hsu, S.-C., Wang, G., Cao, J., Lee, C. S. L., Zhu, L., Chen, Z., Zhao, Y., and Shen, Z.: Chemical characterization and source apportionment of $PM_{2.5}$ in Beijing: seasonal perspective, Atmos. Chem. Phys., 13, 7053-7074, doi:10.5194/acp-13-7053-2013, 2013.

Table 1. Characteristics of Mie lidar

Transmitter			
Laser		Nd:YAG	
Wavelength	532 nm		1064 nm
Pulse energy	130 mJ		130 mJ
Pulse repetition rate		10 Hz	
Pulse width		8 ns	
Beam divergence	0.2 mrad		0.2 mrad
Receiver			
Telescope type		Schmidt Cassegrain	
Telescope diameter		30.5 cm	
Focal length		3048 mm	
Field of view		1 mrad	
Polarization	P and S		None
Number of channels	3		1
Interference filter			
Center wavelength	532.0 nm		1064.1 nm
Bandwidth (FWHM)	0.29 nm		0.38 nm
Transmission	0.66		0 .58
Detectors	PMT		APD
	(Hamamatsu R3234-01)		(EG&G C30956EH)
Signal processing	12bit A/D + Photon counting		
Time resolution	1 min		
Vertical resolution	7.5 m		

Table 2. Characteristics of tropospheric ozone DIAL system

Transmitter					
Pump laser	Nd:YAG				
Wavelength	266 nm				
Pulse energy	107 mJ				
Pulse repetition rate	10 Hz				
Pulse width	8 ns				
Raman active gas	CO_2				
Stokes lines	276 nm	287 nm	299 nm	312 nm	
Pulse energy	7.5 mJ	9.1 mJ	8.4 mJ	No. meas.	
Beam divergence	0.1 mrad				
Receiver					
Telescope type	Newtonian			Prime focus (fiber coupled)	
Telescope diameter	49 cm			10 cm	
Focal length	1750 mm			320 mm	
Field of view	1 mrad			3 mrad	
Interference filter					
Center wavelength	287.2 nm	299.0 nm	312.0 nm	276.1 nm	287.2 nm
Bandwidth (FWHM)	1.02 nm	1.15 nm	0.82 nm	1.07 nm	1.05 nm
Transmission	0.18	0.32	0.36	0.17	0.21
Detectors	PMT (Hamamatsu R3235-01)				
Signal processing	12bit A/D + Photon counting				
Time resolution	1 min				
Vertical resolution	7.5 m				

Figure 1. Mie lidar and ozone DIAL (right) were installed in the container at the left on the ground (left).

(a)

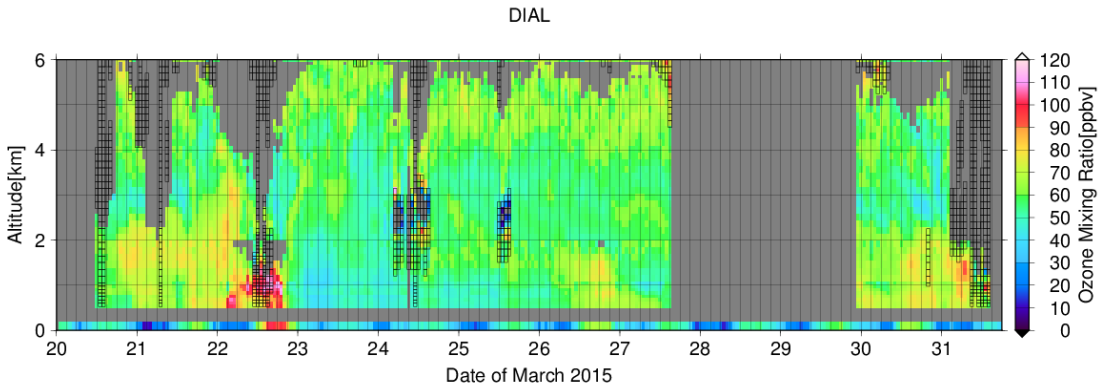

(b)

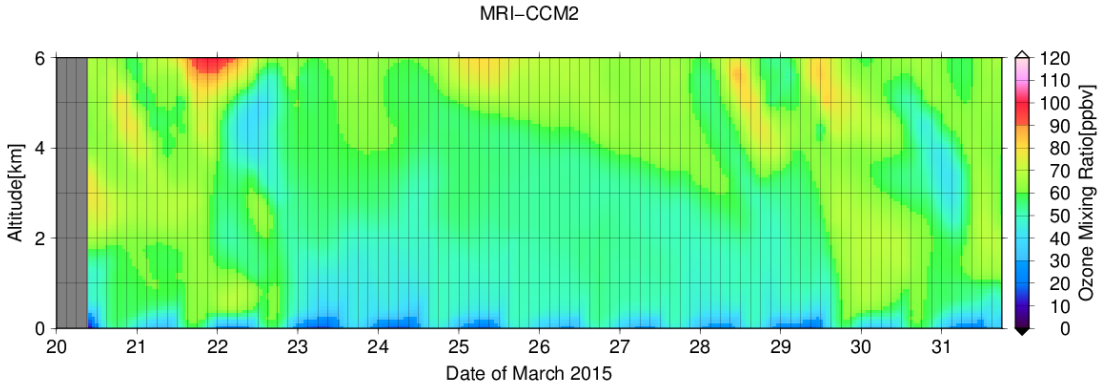

(c)

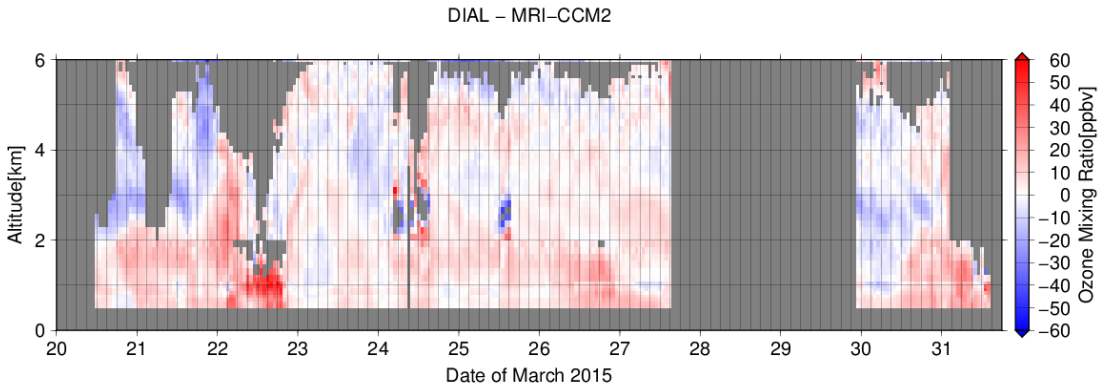

Figure 2. Time-altitude cross-sections of (a) ozone volume mixing ratios observed by DIAL over Saga from 11:10 JST on 20 March to 14:33 JST on 31 March 2015, (b) the ratios simulated by a modified MRI-CCM2 for 20–31 March 2015, and (c) the difference between the observed and simulated ozone volume mixing ratios (a–b). Gray regions indicate areas where there were no observational data or the statistical errors were larger than 10%. Regions enclosed with black rectangles are areas where the data were affected by aerosols and/or clouds. The lowest row in Fig. 2a shows photochemical oxidant (ozone) volume mixing ratios at Takagimachi in Saga city as measured by the Saga Prefectural Environmental Research Center.

(a)

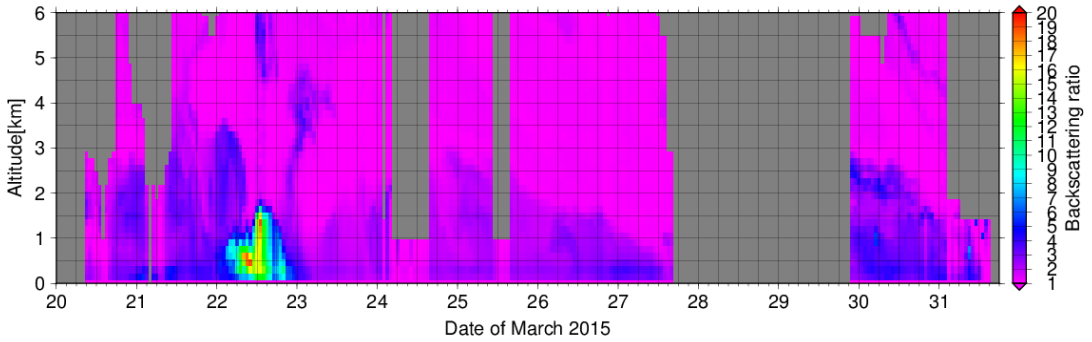

(b) Delete the following chart because the scale of *D* was changed.

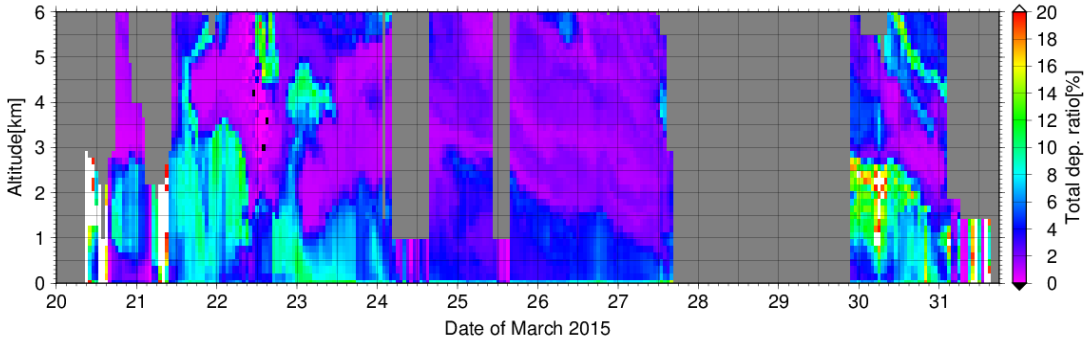

New Fig. 3b

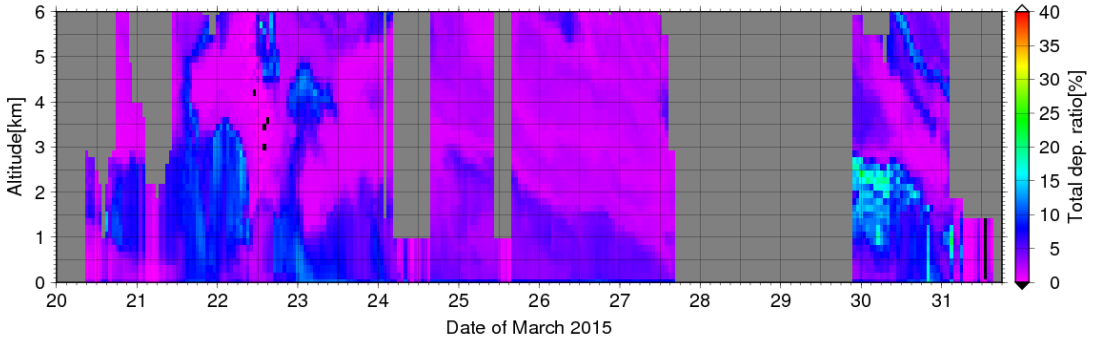

(c)

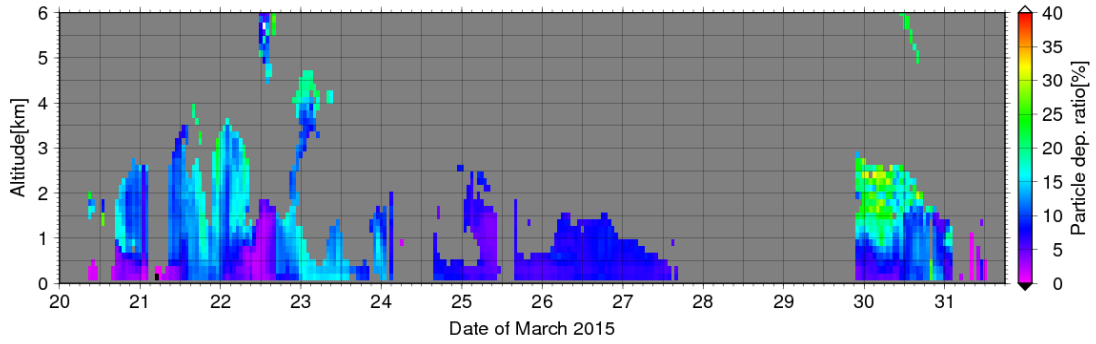

Figure 3. Time-altitude cross-sections of (a) backscattering ratios, ~~and~~ (b) total volume depolarization ratios, and (c) particle depolarization ratios for *R* larger or equal to 2.0 at 532 nm observed by Mie lidar at Saga from 11:10 JST on 20 March to 14:33 JST on 31 March 2015. Lidar observations were not available from 15:56 JST on 27 March to 21:58 JST on 29 March 2015 mainly because of very low clouds and rains~~bad weather~~. Gray regions are areas where there were no observational data or where the observations were affected by clouds.

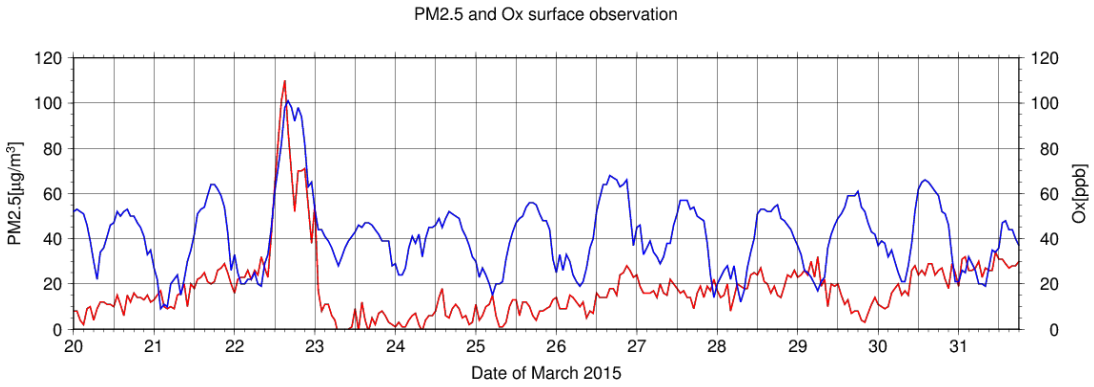

Figure 4. Hourly (JST) data of surface PM2.5 (red line) and Ox (blue line) measured by the Saga Prefectural Environmental Research Center for 20-31 March 2015. The volume mixing ratio of Ox was considered to be that of ozone.

(a)

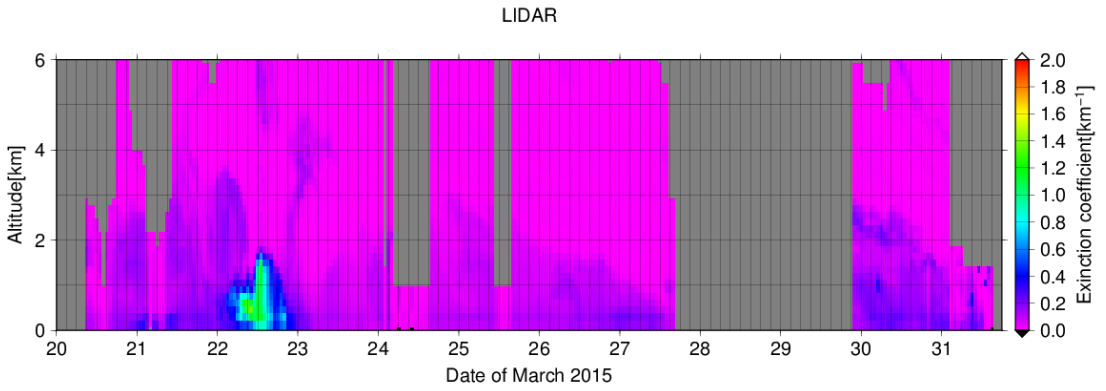

(b)

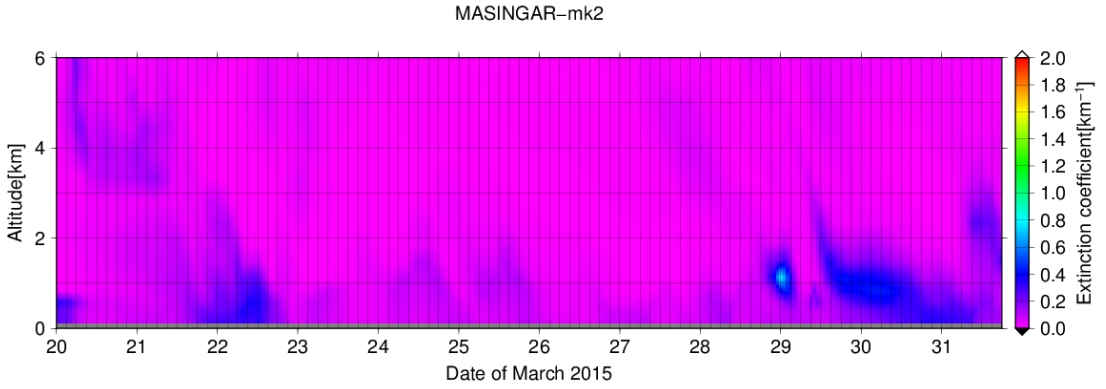

(c)

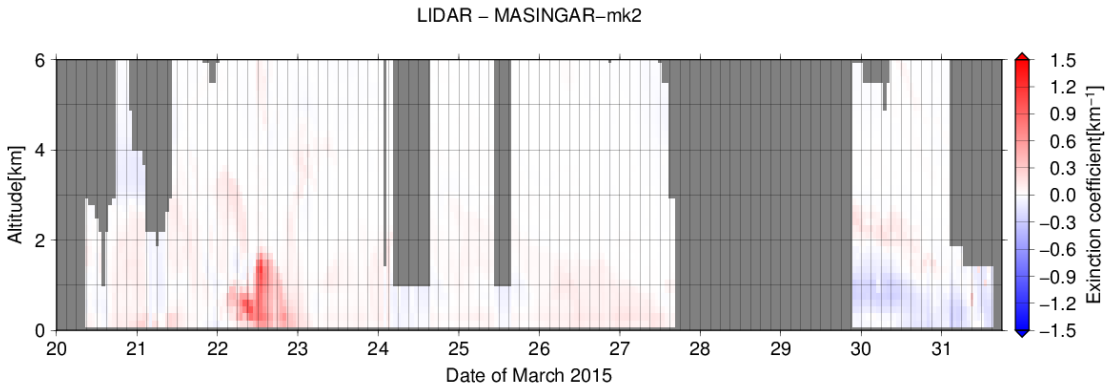

Figure 54. Time-altitude cross sections of (a) aerosol extinction coefficients observed by Mie lidar at 532 nm over Saga from 11:10 JST on 20 March to 14:33 JST on 31 March 2015, (b) the coefficients simulated by MASINGAR-mk2 at 550 nm for 20–31 March 2015, and (c) the difference between the Mie lidar observations and the simulation (a–b). Gray regions represent areas where there were no observational data.

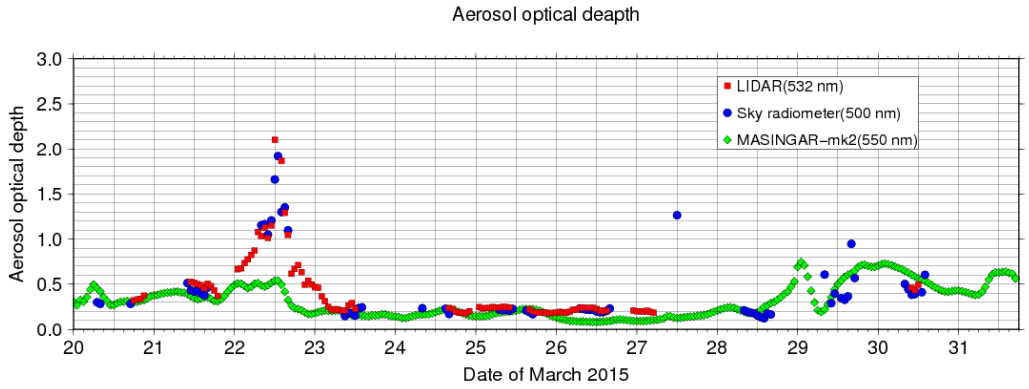

Figure 6~~5~~. Temporal variation of the aerosol optical depth (AOD) measured by Mie lidar at 532 nm (red circles), by sky radiometer at 500 nm (blues circles), and simulated at 550 nm by MASINGAR-mk2 (green circles).

Delete the next figure.

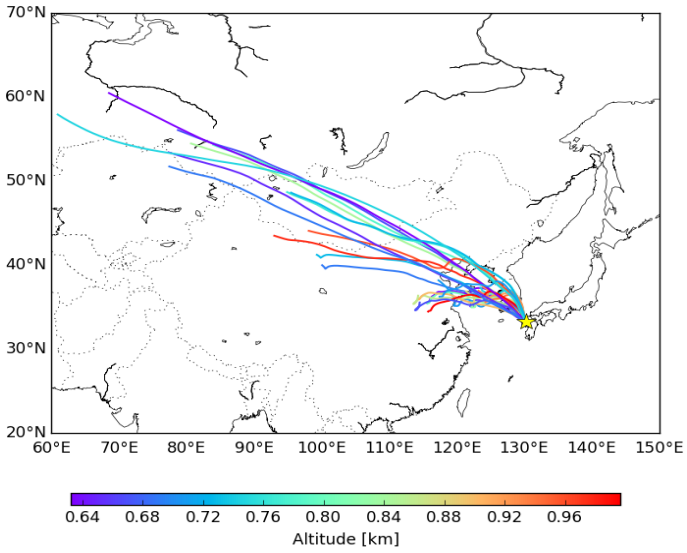

~~**Figure 6.** Horizontal projections of three-dimensional backward trajectories of 27 air parcels initially at altitudes of 600–1000 m over the lidar site at Saga. The colors show the initial positions of the air parcels. The trajectories were calculated for three days from 00:00 UTC (09:00 JST) on 22 March 2015 by the NOAA HYSPLIT trajectory ensemble option using the 1° × 1° Global Data Assimilation System (http://ready.arl.noaa.gov/hypub-bin/trajtype.pl?runtype=archive).~~

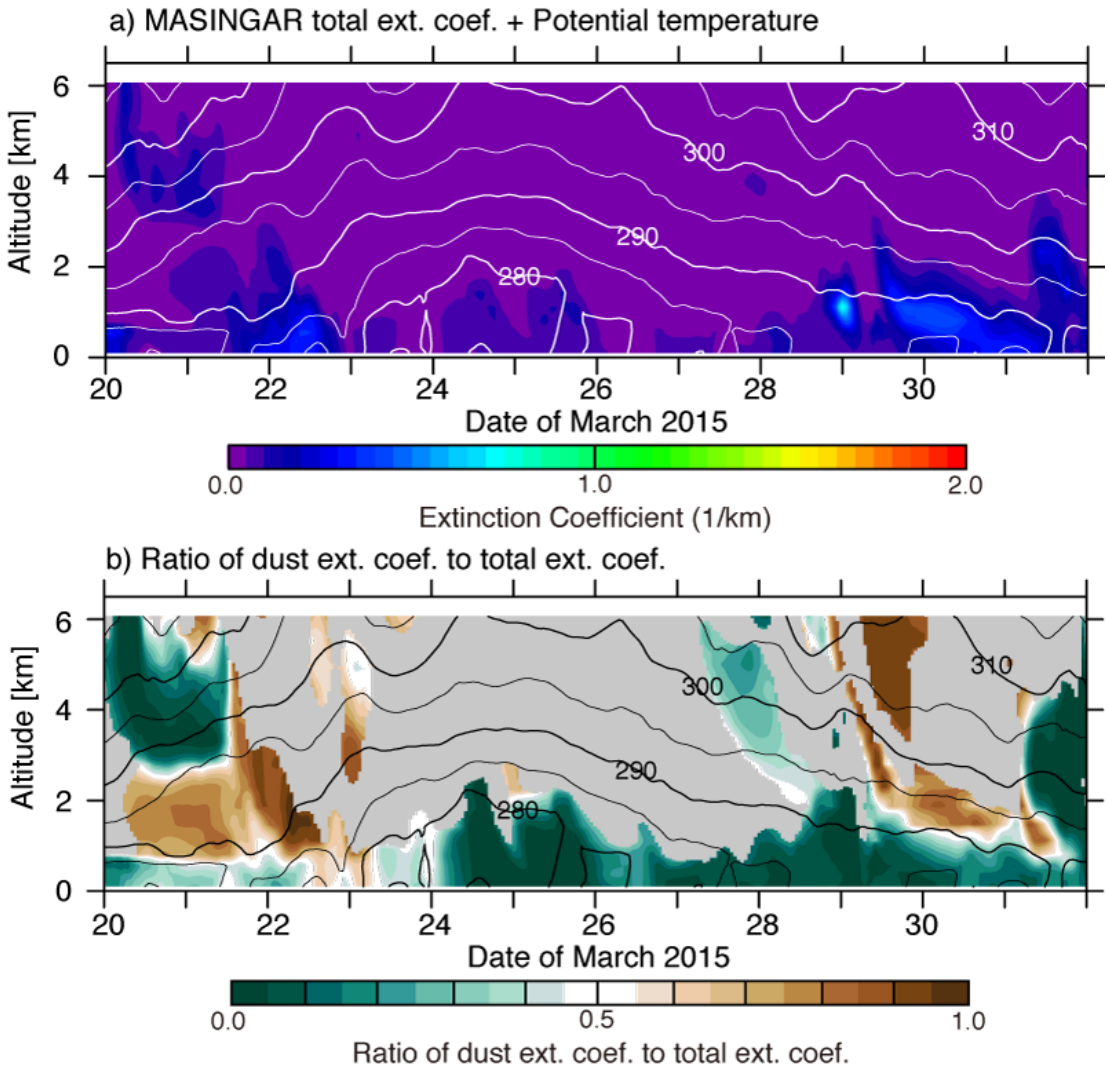

Figure 7. Time (JST)-altitude cross sections of (a) total aerosol extinction coefficients at 550 nm (color shading) and (b) ratios of dust extinction coefficient to total aerosol extinction coefficient (color shading) simulated by MASINGAR-mk2 with potential temperatures (black contours) over Saga for 20-31 March 2015. The gray regions in Fig. 7b indicate that the simulated dust or total? extinction coefficient is less than 0.02.

(a)

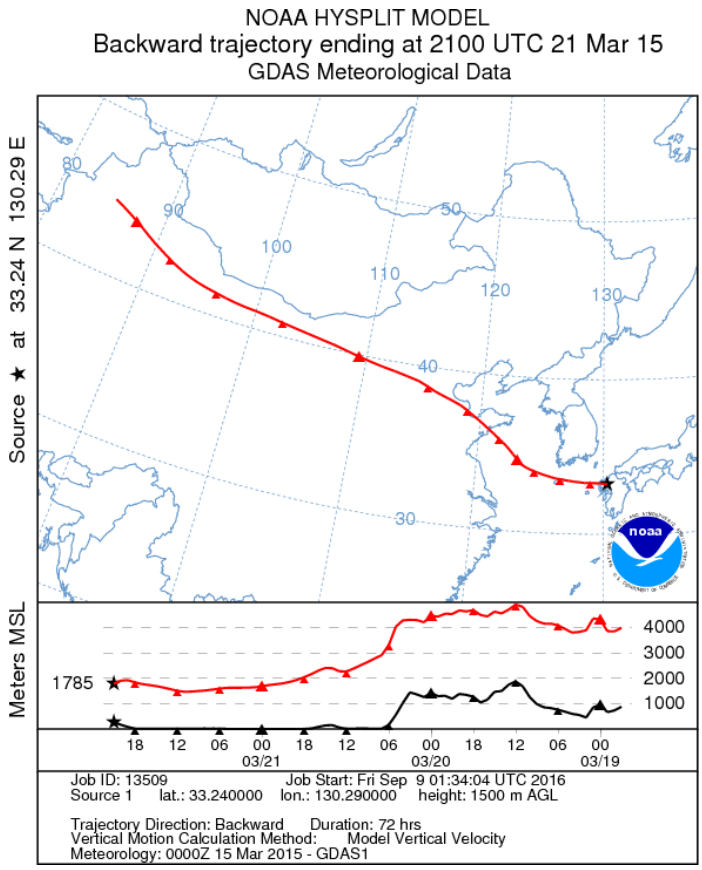

(b)

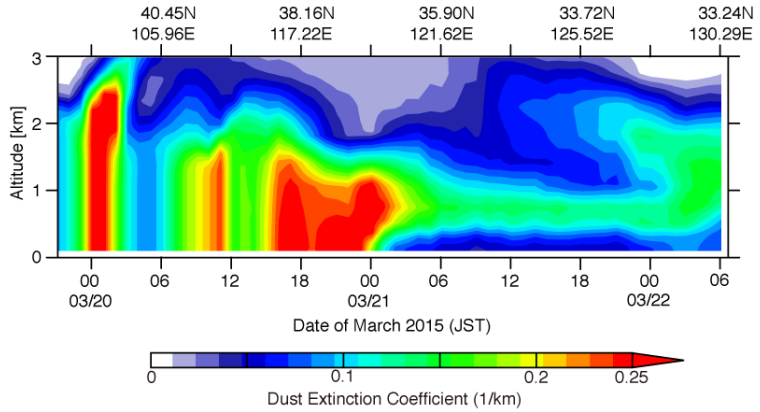

Figure 8. (a) 72-h HYSPLIT-model backward trajectory (red line) and terrain height (black line) from Saga at 1500 m above ground level (AGL) ending at 06:00JST on 22 May 2015. (b) Time-altitude cross section of dust extinction coefficient simulated by MASINGAR mk-2 along the trajectory path.

(a)

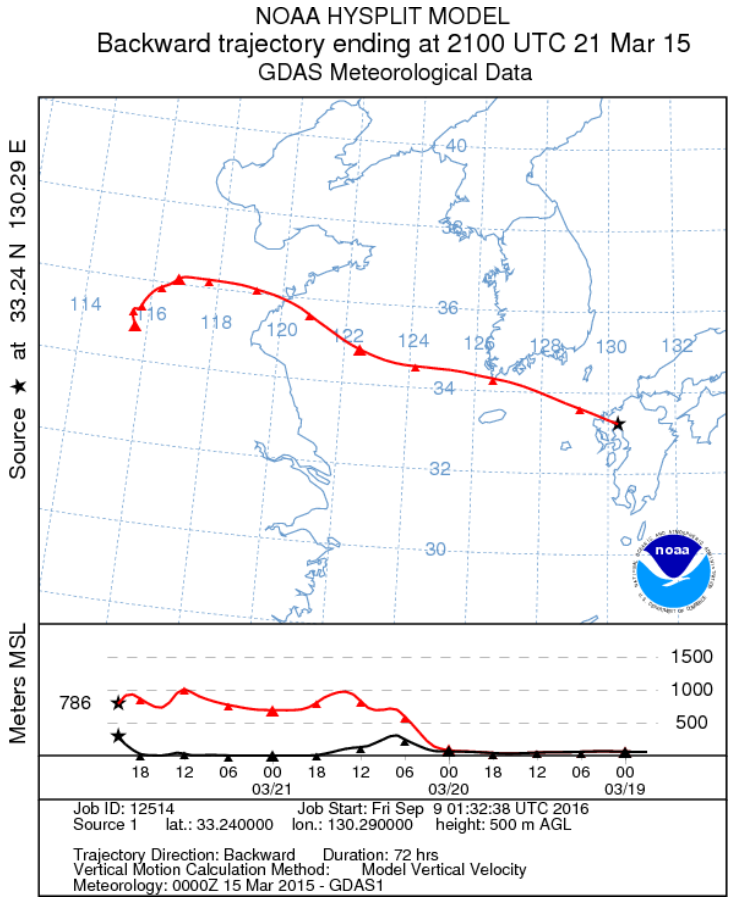

(b)

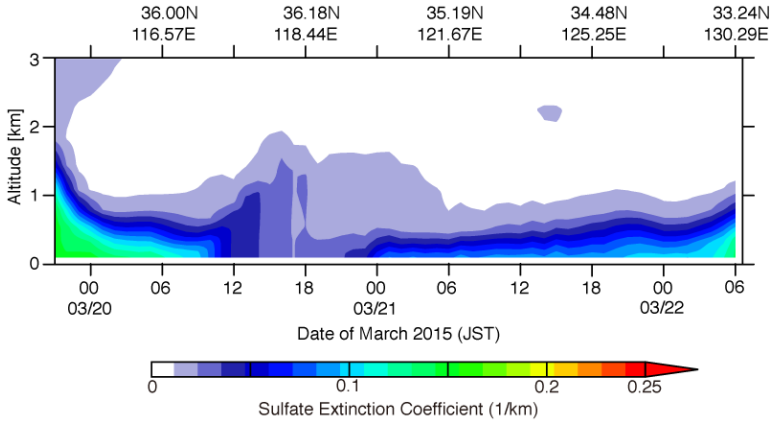

Figure 9. Same as Fig. 8 but for 500 m AGL.

(a) (b)

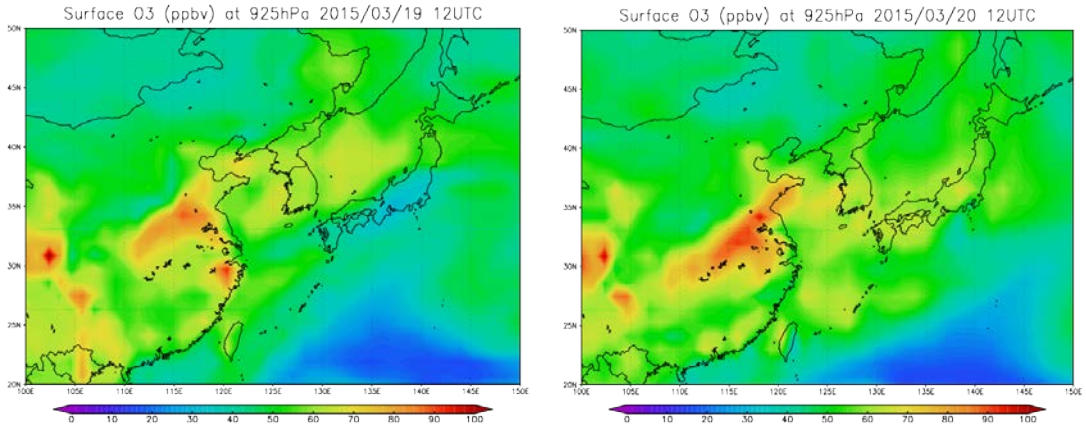

(c) (d)

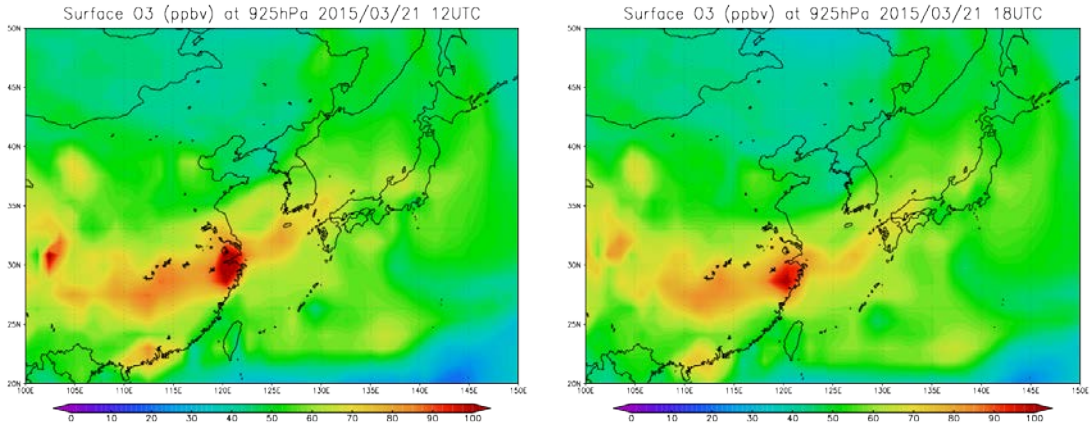

Figure 10. Horizontal maps of ozone volume mixing ratios in ppbv predicted by MRI-CCM2 for 925 hPa pressure level (about 760 m altitude) at 21:00 JST (JST=UT+9) on (a) 19, (b) 20, (c) 21 March and (d) 03:00 JST on 22 March 2015.

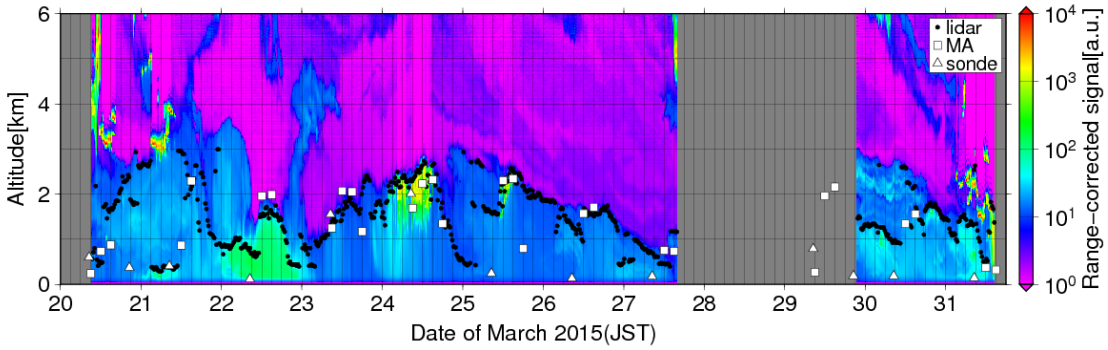

Figure 11. Time-altitude cross section of (color shaded) range-corrected backscatter signal at 1064 nm and the tops of atmospheric boundary layers estimated by Mie lidar (closed black circles), radiosonde (open triangles), and JMA Meso-Scale Meteorological Analysis (open squares) data over Saga from 11:10 JST on 20 March to 14:33 JST on 31 March 2015.